Department of Physics and Astronomy
Heidelberg University

Bachelor Thesis in Physics
submitted by

Paul Vincent Steimle

born in Achern (Germany)

2023

Re-Computation of Precise Radial Velocities of G and K Giant Stars from the Lick Survey with the new Doppler Code pyodine

This Bachelor Thesis has been carried out by Paul Vincent Steimle at the
Landessternwarte in Heidelberg
under the supervision of
Priv.Doz. Dr. Sabine Reffert

Abstract

From 1999 to 2012, the survey of G & K giant stars at Lick observatory in California captured a total of over 15000 stellar spectra at intervals of about one month of 373 stars. The radial velocities (RVs) of those stars have been calculated using the iodine reduction code by Butler et al. (1996). The survey is planned to be continued in the near future with the Waltz telescope at the Landessternwarte in Heidelberg. To analyze these spectra, Heeren (2021) built the "Waltz Data Reduction Software". It features the first open flexible iodine reduction software "pyodine" and is completely written in Python 3. The first step of this work is to provide a proper wavelength solution (WLS) for every observation night, as pyodine needs wavelength calibrated spectra as input. However, for some observation nights, the ThAr spectra do not deliver a good wavelength calibration and therefore, I shift a reference WLS according to shifts obtained from a cross-correlation of iodine spectra. Afterwards, pyodine can calculate the RVs which are in the end compared to the original results as these have proven to be trustworthy. The first tests show that pyodine delivers good RVs that align well with the original results but there is also still room for improvement.

Zusammenfassung

Von 1999 bis 2012 wurden am Lick-Observatorium in Kalifornien insgesamt über 15000 Spektren von 373 G- und K-Riesensternen im Abstand von etwa einem Monat aufgenommen. Die Radialgeschwindigkeiten (RVs) wurden mit dem Jodzellencode von Butler et al. (1996) berechnet. Die Observationen sollen in naher Zukunft mit dem Waltz-Teleskop an der Landessternwarte in Heidelberg fortgesetzt werden. Um diese Spektren zu analysieren, hat Heeren (2021) die "Waltz Data Reduction Software" entwickelt. Sie enthält die erste offene flexible Jodreduktionssoftware "pyodine" und ist komplett in Python 3 geschrieben. Der erste Schritt dieser Arbeit ist die Bereitstellung einer geeigneten Wellenlängenlösung (WLS) für jede Beobachtungsnacht, da pyodine wellenlängenkalibrierte Spektren als Eingabe benötigt. Für einige Beobachtungsnächte liefern die ThAr-Spektren jedoch keine gute Wellenlängenkalibrierung, daher verschiebe ich eine Referenz-WLS entsprechend den Werten, die ich aus einer Kreuzkorrelation von Jodspektren erhalte. Anschließend kann pyodine die RVs berechnen, die schließlich mit den ursprünglichen Ergebnissen verglichen werden, da diese sich als zuverlässig erwiesen haben. Die ersten Tests zeigen, dass pyodine gute RVs liefert, die gut mit den Originalergebnissen übereinstimmen, aber es gibt auch noch Raum für Verbesserungen.

Contents

1 Introduction **3**
1.1 Extra Solar Planet Detection . . . 3
1.1.1 Transit Method . . . 3
1.1.2 Radial Velocity Method . . . 3
1.2 Observation Instruments . . . 5
1.2.1 Lick Survey of K & G Giants . . . 5
1.2.2 Waltz Telescope . . . 5

2 Theory **6**
2.1 Radial Velocity Calculation . . . 6
2.2 Echelle Spectrograph . . . 7
2.3 Iodine Cell Method . . . 8
2.4 Hα Index . . . 8

3 Waltz DRS **9**
3.1 CERES . . . 9
3.2 pyodine . . . 11
3.2.1 Create a Deconvolved Stellar Template . . . 11
3.2.2 Model the Stellar I2 Observation . . . 12
3.2.3 Weight and Combine the Chunk Velocities . . . 12

4 Goal of this Thesis **13**

5 Renaming and Updating the Lick Files **14**

6 Improving the Waltz DRS **16**
6.1 CERES . . . 16
6.1.1 Create Wavelength Solution . . . 17
6.1.2 I2 Correlation . . . 20
6.1.3 Barycentric Velocity . . . 24
6.2 pyhalpha . . . 25
6.3 Run Lick Data . . . 26

7 Results **27**
7.1 Errors . . . 27
7.2 Absolute Residuals . . . 31
7.3 Barycentric Correction . . . 34
7.4 Relative Residuals . . . 36
7.5 Published Stellar Companions . . . 37
7.6 Hα index . . . 39
7.7 Lick Weighting Algorithm . . . 42

8 Conclusion **43**
8.1 Summary . . . 43
8.2 Discussion and Future Prospects . . . 43

9 Acknowledgments **45**

10 References **46**

11 Appendix **49**

1 Introduction

1.1 Extra Solar Planet Detection

From early on, humankind was fascinated by the idea "Are we alone in the universe?". This also raised the question of whether there are other earth-like planets out there somewhere. One of the most formative moments for my interest in astronomy was the news about the discovery of the first earth-like exoplanet in the habitable zone of its host Kepler-186f in 2014 (Quintana et al. 2014). Since the discovery of the first exoplanet (Wolszczan and Frail 1992), a lot of time has passed and more than 5000[1] exoplanets have been confirmed. Although there are numerous ways to detect planets outside our solar system, two methods described as early as 1952 by Russian-American astronomer Otto Struve (Struve 1952) have clearly stood out in the last 20 years: The so-called transit method and the radial velocity or Doppler method.

1.1.1 Transit Method

The transit method is maybe the easiest to describe to a non-physicist. One observes the luminosity of a star and as a planet or planet-like object passes through the optical path between star and observer, the luminosity of the star drops by a few percent or less. If this darkening is observed in a periodic behavior over a longer time span, it is possible that this is due to a planet or companion orbiting the host star. However, to detect an exoplanet with this method, one must observe the star continuously for a very long time period. To date, 3964[1] confirmed exoplanets have been found using this method. The Kepler 0.95m space telescope has contributed the most (2698) to this and is probably the most famous telescope for transits. As the name suggests, Kepler-186f was also discovered with this telescope.

1.1.2 Radial Velocity Method

Until around 2014, the radial velocity (RV) or Doppler method dominated the field of exoplanet discoveries. As the name already reveals, it is based on the RV of the host star and the Doppler shift of its spectrum. If the host star has one or more sub-stellar companions, they will orbit around their barycenter, also called their center of mass. This will lead to small changes in the velocity of the star which then causes small Doppler shifts in its spectrum which then can be detected with high-resolution spectrographs. The movement around the barycenter is governed by gravity, as gravitational pull of both bodies forces them to orbit their center of mass. This reflex motion of the host star is more pronounced for more massive planets, hence it is easier to detect massive planets with small orbits (Fischer et al. 2014).

The RV method relies on several properties of the star, one of them being its mass. As we try to measure absorption lines in order to determine the Doppler shift from them, the star has to have good visible spectral lines. This is only the case for stars with a maximum mass of up to around $1.5M_{\odot}$. The reason for this is that the more massive the star is, the hotter it gets and thus the faster it rotates which will lead to a broadening of the spectral lines until its spectrum will be close to a continuum. In fact, the Iodine Cell Method which will be explained in section 2.3 Iodine Cell Method uses these so-called hot stars for its analysis.

[1] Source: NASA Exoplanet Archive.

One possibility to still find exoplanets of stars with a mass exceeding $1.5\,M_{\odot}$ is to observe the giant stars that left the main sequence of the Hertzsprung-Russel diagram. Some stars on the so-called giant branch are of spectral types G and K. As they evolve and get older, they expand but do not get more massive and so they cool down and their rotation velocity decreases. This then leads to a sharpening of their spectral lines (Wolthoff et al. 2022). One of the telescopes that observed these so-called G and K giants and provided the data that is used in this thesis, is the 0.6m Coudé Auxiliary Telescope (CAT) / 3m Shane Telescope at Lick observatory, located at Mount Hamilton near San José (USA). From 1999 until 2012, the Lick G & K giant survey took around 15.000 spectra of 373 stars[2].

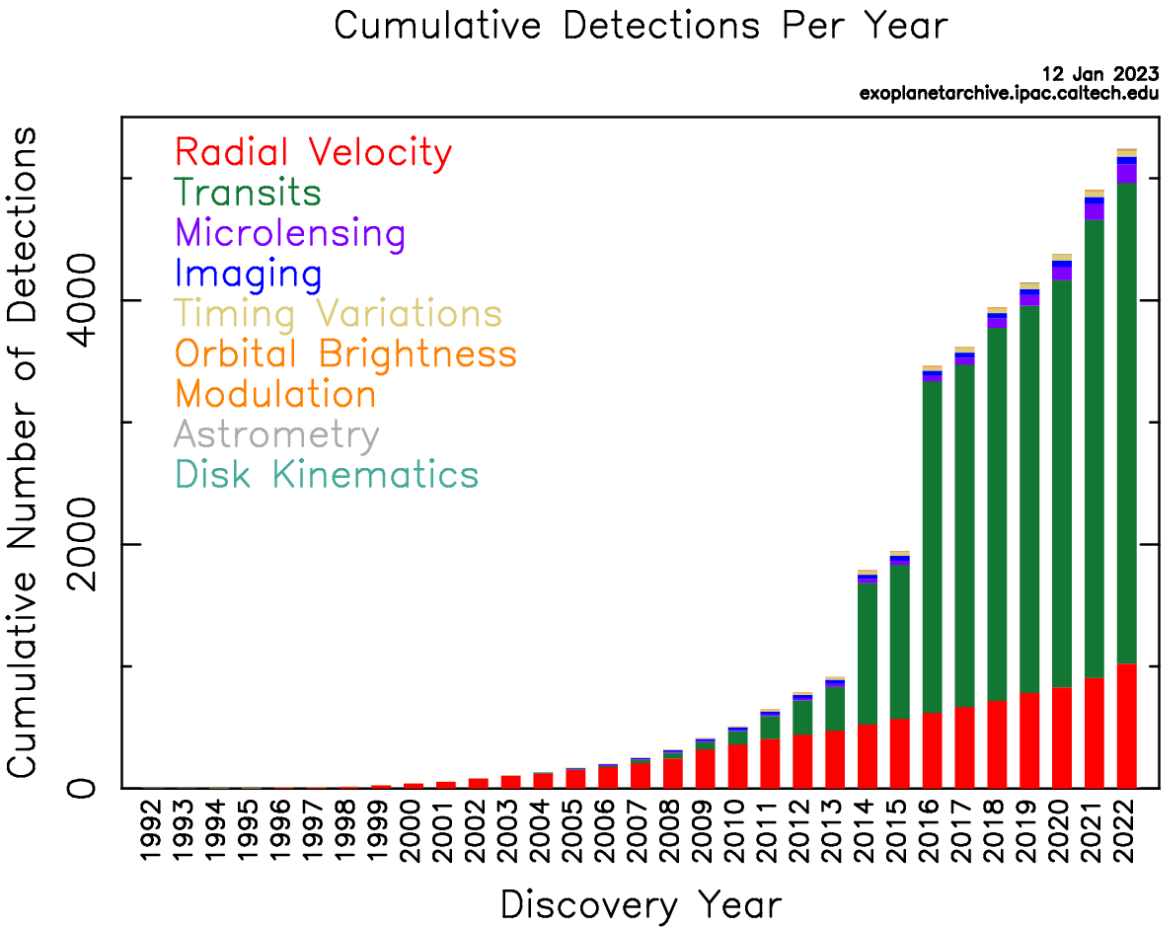

Figure 1: Cumulative count of exoplanet detections indicated by detection method.[3]

[2]Source: LSW Exoplanets.
[3]Source: NASA Exoplanet Archive.

1.2 Observation Instruments

1.2.1 Lick Survey of K & G Giants

The Lick survey of K & G giants (hereafter Lick Survey) was planned in order to provide a sample of stars that could be used as stable grid stars for the NASA Space Interferometry Mission (SIM). For that, these stars had to be astrometrically stable up to around 1μas and could not be part of a multiple system. The observations began in June 1999 with only 86 K giants (Frink et al. 2001). In addition, 96 more K giants were added in 2000 and another sample consisting of 194 G & K giants was included in 2004. Observations were carried out six to eight nights per month with one observation ranging from 30 minutes for faint 6 mag stars to only 5 minutes for bright 3 mag stars (Heeren 2021).
The iodine cell method (Butler et al. 1996) was used to achieve a precision of $3 \sim 8$m/s. This allows to identify stellar binaries as well as planetary companions around the host stars which is what is dealt with in this thesis.
After the discovery of the first exoplanet from the Lick survey Data in the system of ι Draconis, (Frink et al. 2002), a dozen planets, some of which also in multi-planet systems, stellar binaries and brown dwarfs have been found.
In 2012, the I2 cell suffered damage and since the SIM was canceled in 2010, the decision was made to also end the Lick survey. Thereafter, some strong planet candidates were left but in order to confirm or refute them, some extra data was needed. For some stars, it was possible to get further RV measurements with the Hertzsprung SONG telescope on Tenerife (Spain) (Andersen et al. 2014; Franck Grundahl et al. 2008) or with HARPS in La Silla (Chile) (Mayor et al. 2003). But since observation time on public telescopes is rather rare, the search for a dedicated telescope to continue the Lick survey began.

1.2.2 Waltz Telescope

As many of the people that managed the Lick survey worked at the Landessternwarte in Heidelberg (Germany) by then, the Waltz telescope was chosen as the successor.
The 1906-built Waltz telescope is located 568m above sea level at the Landessternwarte (LSW) at the top of the Königstuhl in Heidelberg. As the Waltz telescope is exclusively used for continuing the Lick G & K giants survey, this now allows observations every clear night and hence a bigger statistical survey of G & K giants is planned. Like the Lick, the Waltz uses the I2 cell method to measure precise RVs up to $3 \sim 8$m/s in a non-stabilized environment. Several changes and updates had to be made; most of them in student research. The software for the RV analysis, the so-called Waltz Data Reduction Software, was written by Paul Heeren as part of his Ph.D. thesis (Heeren 2021).
It consists of two main routines: an adapted Python 3 version of CERES (Brahm et al. 2017), which contains routines for the extraction, calibration and wavelength calibration as well as pyodine (Heeren et al. 2023, subm.), which is "an open, flexible iodine reduction software for precise radial velocities".

2 Theory

2.1 Radial Velocity Calculation

In Astronomy, the Doppler shift z is defined as

$$z = \frac{\lambda_{obs} - \lambda_{emit}}{\lambda_{emit}} = \frac{\Delta\lambda}{\lambda_{emit}} = \frac{v}{c}. \tag{1}$$

Here, λ_{obs} and λ_{emit} are the observed and emitted wavelengths, c is the speed of light and v the RV which is defined as the velocity of the star in line of sight to the observer. Since the RV method is mostly interested in the change of the Doppler shift, it is completely free to decide on its rest frame. For most of the time, this rest frame is the one of the template spectrum of the star.

When measuring RVs, one has to correct the result for several influences. The most contributing influence is the motion of the earth with around 30kms^{-1}. Other smaller influences are gravitational time dilation due to objects of the solar system, leap second offset, proper motion and systemic radial velocity of the star, Parallax and Shapiro delay. These so-called barycentric velocity corrections (BVC) are described in Wright and Eastman (2014) and will from now on be summed up to a single barycentric velocity v_B. For the analysis of the barycentric velocities, there are three main components: The first two are the coordinates of the observatory on earth and the coordinates of the star. The third one is the date and time of observation which has to be very precise.

According to Butler et al. (1996), this time of observation has to be known to a precision of around 30 seconds. As the exposure times for some faint 6 mag stars can be up to 30 minutes, it is not very accurate to just take the midpoint of observation. For example, clouds can block some of the incoming light and so the first half of the observation could make up 80% of the collected light. Therefore, a weighted midpoint is introduced. For the Lick as well as the Waltz, this midpoint is calculated via a measurement of incoming photons with a photomultiplier tube.

2.2 Echelle Spectrograph

In order to be used in RV measurements, a spectrograph has to have a high resolution over a wide wavelength range. Hence in astronomy, most of the time an echelle spectrograph (from French échelle, meaning ladder) is used. The theoretical resolution is determined by the wavelength λ and the difference in wavelength $\Delta\lambda$ that can be distinguished at a wavelength of λ:

$$R = \frac{\lambda}{\Delta\lambda} \,. \tag{2}$$

In comparison to a normal grid spectrograph, an echelle spectrograph uses an echelle grating which can be seen in Figure 2 a) as its main dispersion element. For light at wavelength λ that falls onto the echelle grating with incidence angle α, the following applies:

$$n \cdot \lambda = d \cdot (\sin\alpha + \sin\beta) \,. \tag{3}$$

Here, β is the diffraction angle, n the number of the order and d the groove width. For light that is nearly perpendicular to the grating, one can approximate the incidence and diffraction angle to the blaze angle $\Theta_B \approx \alpha \approx \beta$ and so the theoretical resolution of the spectrograph can be written as:

$$R = \frac{\lambda}{\Delta\lambda} = \frac{2\tan\Theta_B}{\Delta\beta} \,. \tag{4}$$

As the highest efficiency is achieved for high blaze angles, the diffraction between orders $\Delta\beta$ is very small. Therefore, most spectrographs have a prism placed after the echelle grating to counter overlapping orders. A graphic of a whole spectrograph similar to the one used in the Waltz telescope and the Hamilton spectrograph can be seen in Figure 2 b).

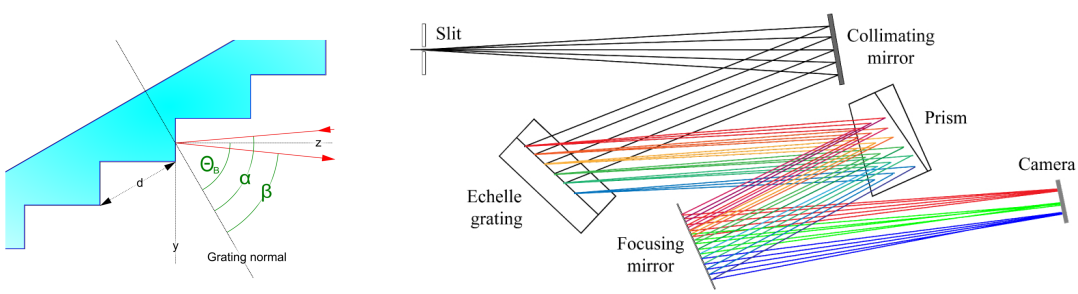

(a) (b)

Figure 2: a) Schematic cross-section of an echelle grating, with blaze angle Θ_B, groove width d, and incidence and diffraction angles α and β.[4] b) Schematic illustration of an echelle spectrograph.[5]

[4] Source: Shen et al. (2018).
[5] Source: Heeren (2021) based on Figure 5.4 in Eversberg and Vollmann (2015).

2.3 Iodine Cell Method

For spectrographs in a non-stabilized environment (temperature, humidity, mechanical, air pressure), small changes can cause large errors in the final RV. In order to correct that, one has to have some sort of reference spectrum. The easiest way would be to make calibrations with for example a Thorium-Argon (ThAr) lamp. However, using a calibration lamp has several downsides. First, the reference and actual science spectrum are not obtained at the same time so there can be changes in the environment even though they might be small. Secondly, the light of the calibration lamp will not take the exact same optical path as the starlight. Hence, there can be some irregularities in the optical components which can lead to errors.

Therefore, another approach can be taken, where a cell containing molecular gas is placed directly in the light path of the starlight so the resulting spectrum will be a composition of the stellar spectrum and the absorption lines of the molecule. In order to make the best use of this, the spectral lines of the molecule have to be in the same wavelength region as the stellar spectrum (around 4000Å to 6000Å). After a long search, molecular iodine has proven to be the best-suited candidate. Even though it only has a spectral range of 5000Å to 6300Å, it brings several advantages in comparison to other candidates. For example, it is non-lethal and has a very high absorption coefficient that allows the cell to measure only around 10cm in length with around 0.001atm of pressure (Marcy and Butler 1992).

2.4 Hα Index

Spectral shifts are usually due to RV changes. However, it is possible that stellar activity can lead to a red- or blueshift in the electromagnetic spectrum of the star. This stellar activity is visible in the photosphere and can lead to spectral shifts that show up periodically as the stellar spots rotate with the period of the star or as an alias of it. Hence, it can be wrongly interpreted as a stellar companion. Fortunately, this effect is relatively small for giants as these show little activity in the photosphere (Heeren 2021).

For G and K giants, the most likely candidate to cause unexplained changes in the RVs so far are non-radial pulsations. Saio et al. (2015) investigates long secondary periods (LSPs) in photometry and their origins with variations of luminosity ranging from 200 to 1500 days. The paper concludes that oscillatory convective modes lead to temperature changes, radial displacement, and density variations. These oscillatory convective modes have an effect on the depths of absorption lines and hence change the measured RVs. To analyze this effect, one can take a separate look at the spectral lines of the star. For giants, the Hα line is very distinct. Staudt (2020) developed a Python 3 package `pyhalpha` based on the Hα index analysis of Boisse et al. (2009). The package was later implemented into the Waltz DRS by Hirschbeck (2022).

The Hα index Hα_{ind} is calculated via the integral over the Hα spectral line at 6562.808Å (in air) divided by the sum of the continuum at the left F_r and right F_l:

$$\text{H}\alpha_{\text{ind}} = \frac{F_{H\alpha}}{F_r + F_l} \,. \tag{5}$$

3 Waltz DRS

To obtain RVs from stellar spectra, the echelle orders have to be extracted and a rough wavelength solution has to be applied. In the second step, the real RV calculation is done via forward modeling of a template spectrum.

3.1 CERES

The first part of the Waltz Data Reduction Software (short Waltz DRS) is a modified Python 3 version of CERES, a **C**ollection of **E**lemental **R**outines for **E**chelle **S**pectrographs (Brahm et al. 2017). It contains all necessary reduction and calibration routines to obtain a so-called reduced spectrum. For that, several calibration and reference spectra have to be taken before, during and after the observations. These are Biases, Darks and Flats that are also used for "normal" astronomic image processing, as well as some wavelength calibration spectra, in most cases spectra from a ThAr lamp.
For Darks and Biases, the image processing is the same as with other astronomical observations. Thereafter, the orders are extracted in two steps. As the echelle orders span over several pixels in cross-dispersion direction on the CCD detector as can be seen in Figure 3, these orders are being traced and then summed up over pixel columns in cross-dispersion direction to get a one-dimensional spectrum. As the inner pixels of an order have a higher intensity and hence a higher S/N, a simple sum over the pixel would not lead to a maximum in S/N. Hence, the first simple extraction step is followed by a second one using the weighting algorithm of Marsh (1989), which is based on Horne (1986) but improved for distorted spectra.
These weights are computed by using the the Masterflat, which is a sum of all single Flats, as input. This optimal extraction is then done for ThAr, I2, and science spectra. Now the extracted Masterflat is used to correct for pixel to pixel variations, dust and distortions in the optical path. After that, the continuum of the spectrum is fitted to obtain a normalized intensity. The last step then is to estimate a rough wavelength calibration from the ThAr spectra. This is done by using a so-called wavelength atlas which contains information about the spectral lines and their corresponding laboratory wavelength. The atlas is fitted via defining the shifts and scaling factor by a cross correlation function. In the end, CERES saves all the spectra as FITS files in a designated folder. These FITS files have 4 or 9 dimensions, depending on the format one chooses. These dimensions contain for example the flux values, the wavelengths, the continuum or their errors (Heeren 2021).

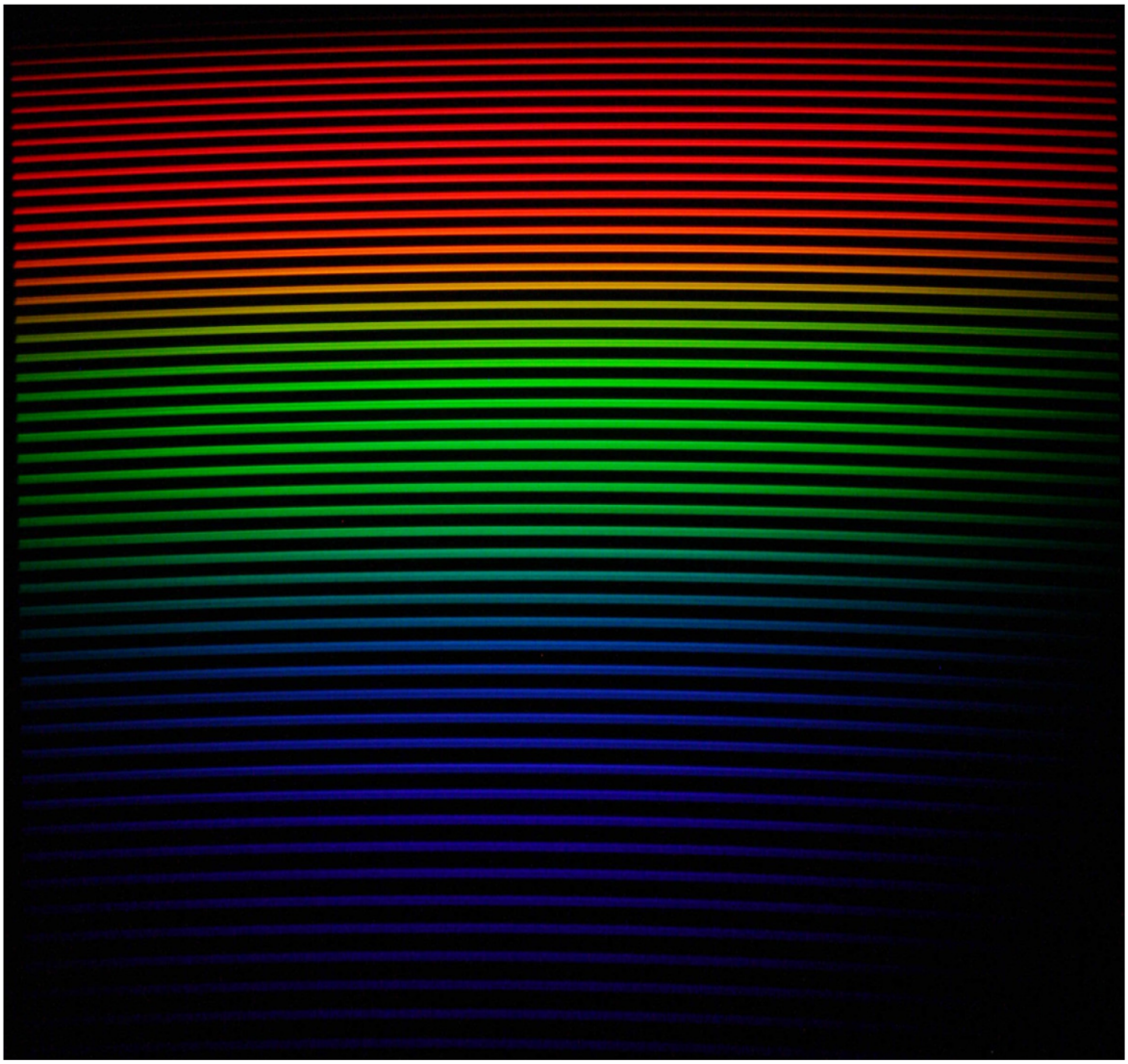

Figure 3: Echelle spectrum of a halogen lamp, obtained with a DSLR camera in the laboratory.[6]

[6]Source: Heeren (2021)

3.2 pyodine

Pyodine (Heeren et al. 2023, subm.) was originally written by René Tronsgaard Rasmussen (Rasmussen 2016) as an alternative to iSONG but was never completely finished. Hence, it is based on the iSONG code dedicated to the Hertzsprung SONG in Tenerife (Spain) (Antoci et al. 2013; F. Grundahl et al. 2017). Paul Heeren completed the project, keeping it highly modular to be easily adaptable to different telescopes that use the I2 cell method. It is the first public flexible iodine reduction code, completely written in Python 3, and includes adaptations to the SONG, Waltz and Lick telescopes. The main routines can be split up into three different parts.

3.2.1 Create a Deconvolved Stellar Template

The first part is the template creation. This template acts as a reference frame, is used for modeling the stellar I2 spectra and is only created once per star. The routine is based on Marcy and Butler (1992) and allows one to identify the line spread function (LSF) $L(x)$. Here, $L(x)$ is a model of the LSF which consists of a central Gaussian accompanied by several satellite Gaussians on the left and right in order to provide a high flexibility. To create the template, three inputs are needed.
First, a high resolution spectrum of the I2 cell $T_{\mathrm{I2}}(\lambda)$. This is normally taken in a laboratory with a Fourier transformed spectrum (FTS) and only has to be done once. And one also needs a so-called template spectrum for every star together with several hot star spectra. These are taken during observation with hot star spectra directly before and after the template spectrum. Here, the stellar template spectra $\hat{I}(x)$ are obtained without the iodine cell and the hot star spectra are observations of O or B stars with the I2 cell. The idea behind this is that these hot star spectra contain only the I2 lines convolved with the LSF as the hot stars show no absorption lines due to their high temperature. By modeling

$$\hat{I}(x) = k(x)\, T_{\mathrm{I2}}(\lambda(x)) * L(x)\,, \tag{6}$$

(Heeren et al. 2023, subm.) where k is the continuum, x indicates the pixel and $\lambda(x)$ is a model of the wavelength scale in the chunk, one can obtain the LSF $L(x)$. To keep the model as simple as possible, the whole spectrum is split up into chunks of around 2Å which typically corresponds to around 40 to 60 pixels. Finally, the stellar template spectrum $\hat{I}(x)$ can be "cleaned" from the LSF through a deconvolution of

$$\hat{I}(x) = T_*(\lambda(x)) * L(x) + N(x) \tag{7}$$

(Heeren et al. 2023, subm.) and we obtain the "true" deconvolved stellar template spectrum $T_*(\lambda(x))$.

3.2.2 Model the Stellar I2 Observation

In the second step, the normal stellar observations $\hat{I}_{\text{obs}}(x)$ that are obtained with the I2 cell are modeled to the template:

$$\hat{I}_{\text{obs}}(x) = k(x)\left[T_{\text{I2}}(\lambda(x)) \cdot T_*(\lambda(x) \cdot (1+z))\right] * L(x) \tag{8}$$

(Heeren et al. 2023, subm.). Here, z denotes the astronomical Doppler shift. The modeling is performed using a Levenberg-Marquardt non-linear least-squares approach, again on spectrum chunks of 2Å in length. Then, the resulting chunk velocities in Dopplershifts z are converted into velocities v_i and saved.

3.2.3 Weight and Combine the Chunk Velocities

Lastly, the chunk velocities are combined into one single final RV. The easiest way to do this is to simply take the median over all chunks of a given observation $RV = \bar{v}_i$. However, this is not the optimal way as the amount of relevant absorption features differs greatly between chunks, as well as the S/N and influence of errors and systematics such as cosmics.

One way is to sort out outlier chunks by certain criteria such as chunk velocities, minimal counts in a chunk or the χ^2_{red} of the chunk fits. This approach was used in the original code with which the Lick RVs were calculated. This original filtering is also implemented in pyodine and called Lick weighting hereafter. Another way would be to calculate weights for the chunks.

Pyodine's main weighting algorithm is similar to the one used in the iSONG code (SONG weighting hereafter). Here, pyodine uses a complex chunk weighting algorithm that takes into account not only a single observation but all possible observations of the star. This then results in a 2D matrix ($n_{\text{obs}} \times n_{\text{chunks}}$) of velocities v_{ij}. Refer to Heeren (2021) for a full description of these algorithms, as they go beyond the scope of this thesis.

As the resulting velocities still contain the barycentric velocity, pyodine then corrects this by using the Python 3 package `barycorrpy` (Kanodia and Wright 2018), which is based on the IDL algorithm `barycorr` by Wright and Eastman (2014).

4 Goal of this Thesis

As Hirschbeck (2022) points out, pyodine has problems with calculating RVs for every stellar spectrum in the Lick G & K giants sample. For example, in Figure 8 of Hirschbeck (2022), the time series of HIP75458 with pyodine RVs and original RVs is plotted. One can see that for around 50% of the original RVs, the pyodine RVs are missing. The reason for that is that the Waltz DRS, more precisely the Python 3 version of CERES in the Waltz DRS, is not able to apply a good wavelength calibration.

This work focuses on a complete re-computation of radial velocities from spectra of G & K giant stars obtained at the Lick Observatory, hence one must first provide a good wavelength solutions (WLS) for each observing night. This is done by improving the part of CERES where the WLS is obtained from ThAr spectra and by shifting the WLS based on a cross-correlation of I2 Flats. Pyodine is then tested on the whole set of observations from the Lick survey and compared to the original results. These were calculated with the Doppler code from Butler et al. (1996), which has proven to deliver trustworthy results. This will help to better assess the performance of the Waltz DRS.

Additionally, there are also some advantages of a homogeneous pipeline like the Waltz DRS, especially for double stars with long periods, where you cannot fit a good offset. Here, the new reduction is essential. Heeren (2021) also pointed out that a re-analysis of the Lick spectra might lead to new astrophysical insights where the new RVs differ from the original RVs.

5 Renaming and Updating the Lick Files

The Lick spectra were recorded in so-called runs which were named from s01 to t70. A run usually consisted of three to five observation nights with one logsheet corresponding to each night. The actual files were named sequentially throughout the run, starting at 1. However, since a uniform database for the LSW is planned for the future, it was decided to use a different naming convention from now on. The observation night folder will be named with the date of the start day following the format YYYYMMDD. The individual spectra are first given a lowercase letter indicating the telescope, e.g. "l" for Lick or "w" for Waltz. Then follows the start date of the observation night along with a sequential number starting at 00001. This then results in the complete file name, for example l19990101_00001. To distinguish between raw spectra and reduced spectra, the latter is preceded by an r in the file name.

Along with this renaming, I fixed some issues with the FITS headers of the files:

First, I corrected the entry for `FILTER` that sometimes consisted of non-UTF-8 characters which then caused an error when loading the FITS header with astropy. This is maybe due to the conversion of the Lick files from their original ".ccd" format to the now uniformly used ".fits" format (Hirschbeck 2022).

Another listing that caused errors was the mid-time `MPMID` that is used for the barycentric correction. For some spectra, this was wrong; for example, the mid-time was after the stop time. According to my supervisor Sabine Reffert, this was due to a problem with the network connection. The mid-times were also listed correctly in the logsheets, as this was the only relevant resource for the original pipeline. Therefore, I decided to introduce a new header entry called `MID-LOG` which consists of the mid-times from the logsheets and changed the part in pyodine where this is read in.

Along with this, I decided to correct some entries in the `OBJECT` header with the entries from the logsheets. Some of them were simply missing or just contained "HIP" without the number which then caused errors in CERES and pyodine as without a HIP number, the spectrum will not be used. If the logsheet entry was "junk", I also corrected the header, as this causes pyodine not to consider these files for analysis.

Besides the mid-time and the star name, there is a different input needed which is the location of the observatory. For the Lick as well as the Waltz and SONG Hertzsprung, the coordinates are saved in a dictionary. The function `get_instrument` in `load_pyodine` determines the instrument depending on header entries. For example for the Waltz, it just scans for "Waltz" in the header entry `TELESCOP`. Unfortunately, for the Lick there was no uniform entry and so pyodine searches for different texts in several positions, one of them being "Hamilton" in `INSTRUME`, and even with this, for some files, it still found no fit. Hence, I decided to create the header `INSTRUME` with the entry "Hamilton" in all Lick files that did not have such an entry.

As for the original Lick reduction pipeline, the spectra always had to be of the same format. For example, the Hα spectral line had to be in order 28 to not cause errors. Since the order position on the CCD can change depending on factors like humidity, temperature or air pressure, it could happen that

the orders were shifted so significantly that one order was added or dropped at the bottom of the sensor. If this was the case, the spectra were simply shifted to the right place after the extraction. Unfortunately, as this was done by hand, sometimes only the science spectra were corrected and the ThAr and I2 were left in the original as they were not needed. The Waltz DRS, however, can handle such shifts and as the ThAr as well as the I2 files were needed for the analysis in this thesis, I decided to undo this shift.

6 Improving the Waltz DRS

6.1 CERES

Hirschbeck (2022) already showed that pyodine is not able to calculate RVs for every stellar spectrum of the Lick sample. As it seems, the main reason for that is that CERES is not able to provide good WLS for some spectra. To create a WLS, CERES fits a ThAr wavelength atlas to the ThAr spectrum via a cross-correlation function (CCF). In order to estimate the quality of a WLS, the code returns a parameter called WLS precision $\mathrm{WLS_{prec}}$. It is the rms (root-mean-square) of the residuals between the wavelength of the ThAr lines in the atlas and their corresponding wavelength in the spectrum, converted to the velocity space. This means that a precision of $50\,\mathrm{ms}^{-1}$, from which I consider a WLS as good, corresponds to a rms of around 0.001 Å.
In order to get a first view of the problem, I updated the function that saves the WLS parameters (e.g. $\mathrm{WLS_{prec}}$) to a text file in such a way that the data is now written into a table to be easily machine-readable.

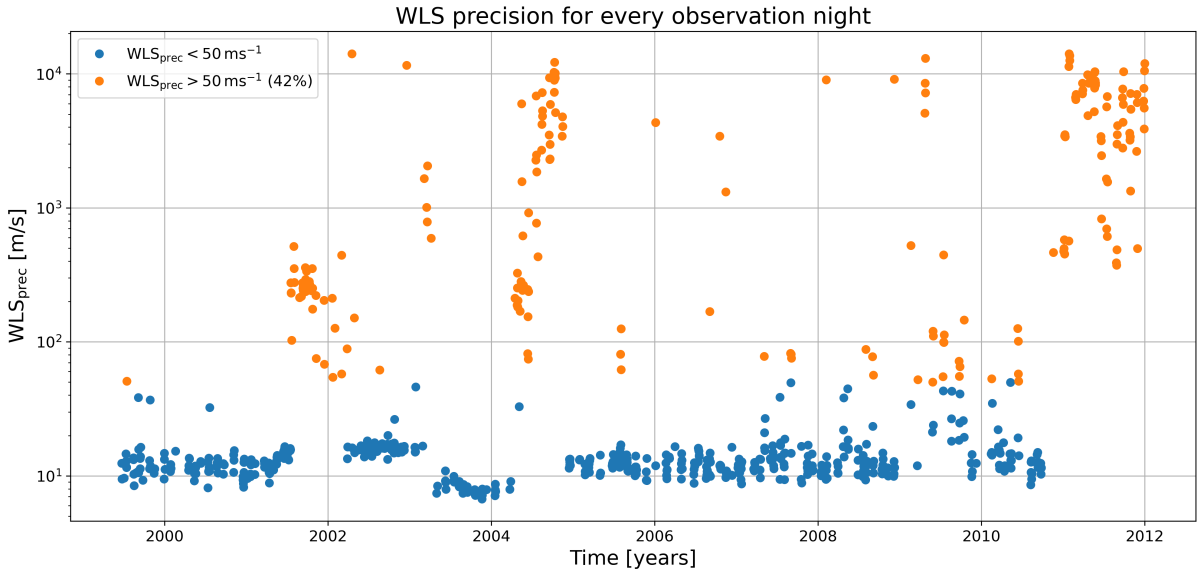

Figure 4: Precision of the WLS of every observation night of the original CERES_lick script from Heeren (2021). For all values below $50\,\mathrm{ms}^{-1}$, a good wavelength solution can be obtained. Good WLS with a precision of $< 50\,\mathrm{ms}^{-1}$ are color-coded in blue, bad WLS $> 50\,\mathrm{ms}^{-1}$ in orange.

After that, I started to split up CERES into different sub-functions like `calculate_wavelength_solution`. This takes only the `reduction_parameters` object along with an input ThAr-file, creates a wavelength solution and returns it along with the optimal parameters which are needed for applying the WLS to the spectra. The function `apply_wavelength_solution` then applies a WLS saved in a ".h5" file to all spectra in this observation night.

6.1.1 Create Wavelength Solution

Along with restructuring, I encountered that for the WLS, just the first ThAr spectrum of the observation night was used. Hence, I implemented a loop over all ThAr spectra of a night and filtered out the one with the best `WLS_prec` for use. When comparing Figure 4 with Figure 5 (top), one can see that this already improved things a bit, as there are now only 33 % of the WLS with an $\mathrm{WLS_{prec}} > 50\,\mathrm{ms^{-1}}$ in contrast to the original 42 %.

Together with the $\mathrm{WLS_{prec}}$, I plotted the order shift as well as the shift in dispersion direction as these two are the main parameters to fit the ThAr atlas to the spectra and hence the precision of the WLS is dependent on them. As can be seen in Figure 5, there might be some correlation between the bad precision of the WLS and the big shift in dispersion direction around 2002 and shortly after 2004.

By restructuring CERES, I changed the way the object that contains all parameters is used. Originally, the input parameters are fixed as the object is newly loaded for every observation night, whereas in the restructured version, the input parameters are the optimal parameters of the night before. This improved the overall percentage of observation nights with a $\mathrm{WLS_{prec}}$ lower than $50\,\mathrm{ms^{-1}}$ from 33 % to 19 %. However for some nights, it produced worse results. The reason for that is that with the "free" parameter object, the orders in which the cross-correlation is done can change. As it turned out, the cross-correlation was only done for one atlas order with several orders of the spectrum. The atlas order was dependent on two parameters. Hence, as WLS creation routine is able to change these two, this resulted in different outcomes for RV precision of the WLS.

I adapted the code so that now always the same three atlas orders are correlated with the same eleven orders of the stellar spectra. For each order combination, the CCF value is stored and at the end, only the shift in dispersion and cross-dispersion direction from the highest CCF value is taken for the creation of the WLS in order to ensure that not one atlas order is identified with several orders from the ThAr. The default value for a maximum shift in dispersion direction was originally set to ± 10 pixel. I changed this value during my work with CERES several times and as the final result (Figure 6 bottom) as well as Figure 5 (bottom) show, 5 pixel is sufficient to cover most of the good ThAr spectra. Figure 5 reveals that there could be a wrong CCF maximum for several spectra with dispersion shifts greater than 5 pixels. Therefore, I changed the maximum value for a shift in dispersion direction to $5\mathrm{ms^{-1}}$ to rule this out.

For some observation nights, the logsheets contain information about a bigger shift in dispersion direction (up to 30 pixels). Consequently, the maximum dispersion shift of only 5 pixels is not sufficient for these spectra to provide a good WLS. I additionally implemented another exception: when the best $\mathrm{WLS_{prec}}$ of an observation night is not below $50\,\mathrm{ms^{-1}}$, another cross-correlation of all ThAr spectra with the maximum shift in dispersion direction set to 35 pixels is done. The final result is shown in Figure 6. As one can see, nearly all ThAr spectra before 2011 deliver a sufficient WLS with a precision of $< 50\mathrm{ms^{-1}}$, in total 86 %. However, especially spectra after 2011 result in a bad WLS precision of up to $10^4\mathrm{ms^{-1}}$. For these last 14 %, one must use a different method.

Figure 5: Precision of the WLS (top), order conversion factor (middle) and shift in dispersion direction (bottom) of every observation if the best ThAr spectra of the night is used. Good WLS with a precision of $< 50\,\mathrm{ms}^{-1}$ are color-coded in blue, bad WLS $> 50\,\mathrm{ms}^{-1}$ in orange.

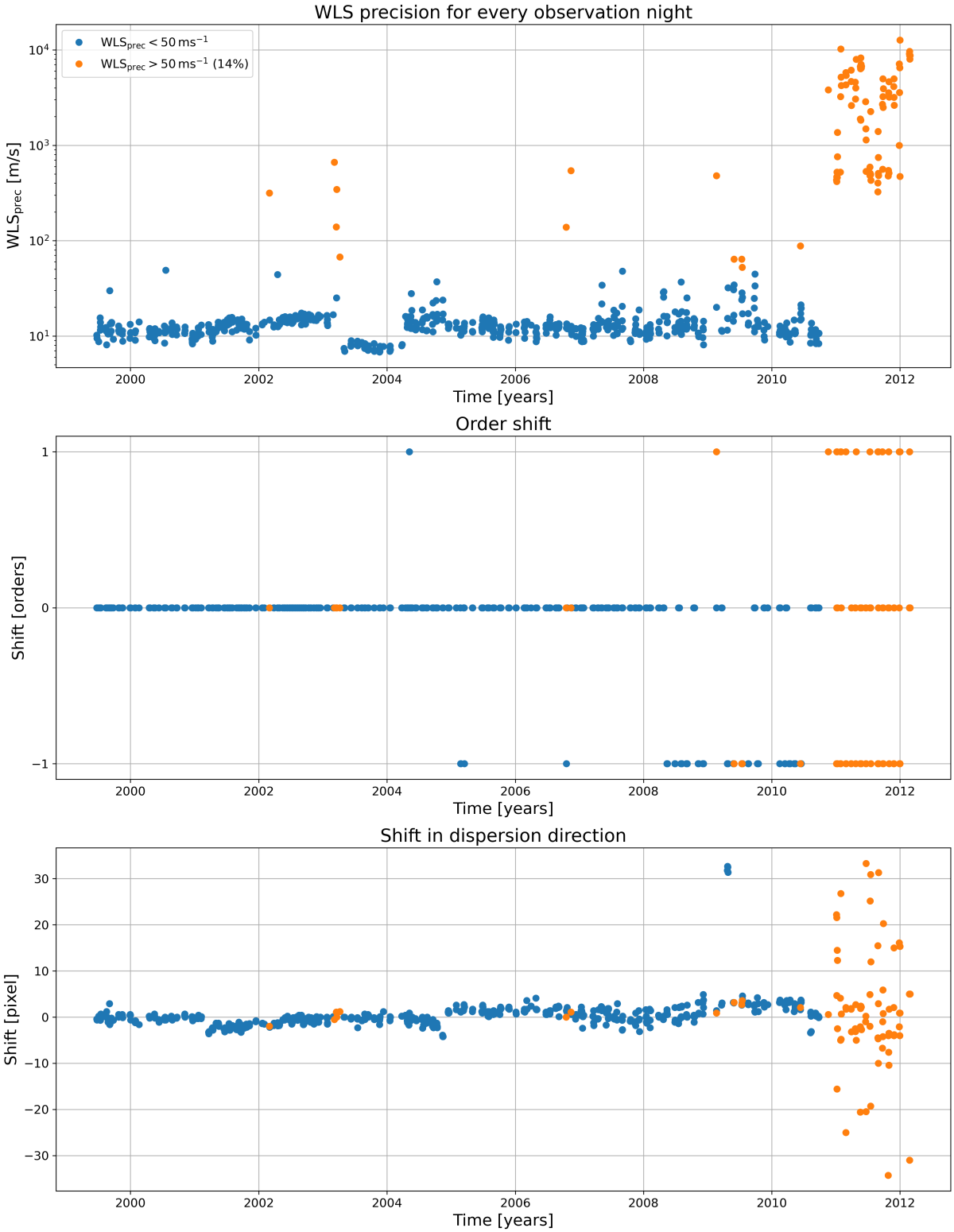

Figure 6: Final $\mathrm{WLS_{prec}}$ (top), order conversion factor (middle) and shift in dispersion direction (bottom). Good WLS with a precision of $< 50\,\mathrm{ms}^{-1}$ are color-coded in blue, bad WLS $> 50\,\mathrm{ms}^{-1}$ in orange.

6.1.2 I2 Correlation

As Figure 6 shows, the updates in the WLS section of CERES improved the results a lot already, but especially for all nights after around the start of 2011, there was still room for improvement. In Figure 7, two ThAr spectra are shown. The top one from 23rd of August 1999 results in a good WLS with a precision of around 10ms^{-1}, the bottom one taken on the 30th of December 2011 produces a WLS with a precision of over 6000ms^{-1}. Reasons for the bad precision of the WLS could be the numerous hot pixels in order 40 to 60 or also the blurred spectral lines at the bottom.

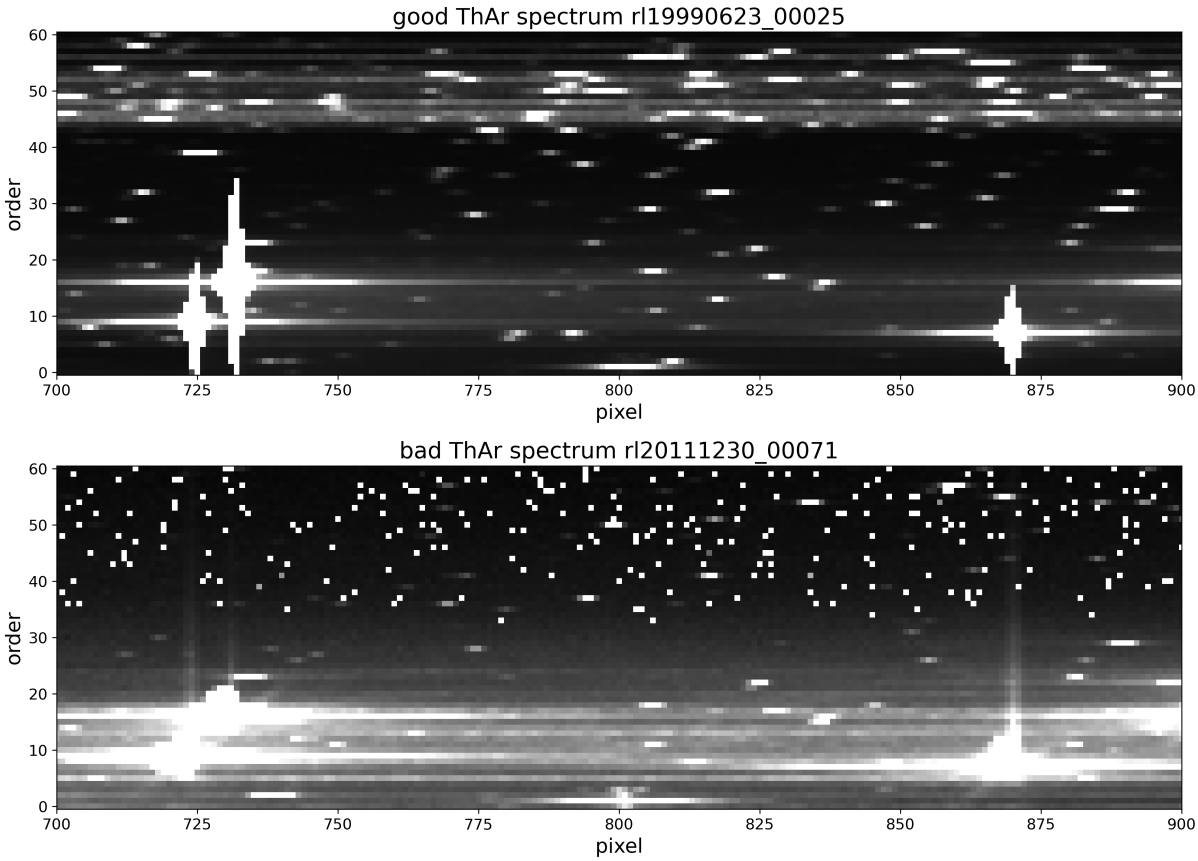

Figure 7: Top: good ThAr spectrum with a WLS_{prec} of $< 50\text{ms}^{-1}$. Bottom: bad ThAr spectrum with a WLS_{prec} of $> 50\text{ms}^{-1}$. The intensity is color coded, black displays a low photon count and white a high count of up to 2000 for the top one and 5000 for the one at the bottom.

Hence, another solution had to be found, which is the usage of the I2 Flats that are recorded for every observation night. These I2 Flats are normal Flats from a halogen lamp but with the I2 cell in the light path. Via a cross-correlation of an iodine spectrum of a night with a good WLS and one where the WLS is not sufficient, the dispersion and cross-dispersion shift are determined. In CERES, this is done with the function `correlate_i2s` by using `scipy.signal.correlate2d` in the "valid" mode. As the CCF is only defined on integers, a Gaussian is fitted to determine the exact shift in the dispersion direction.

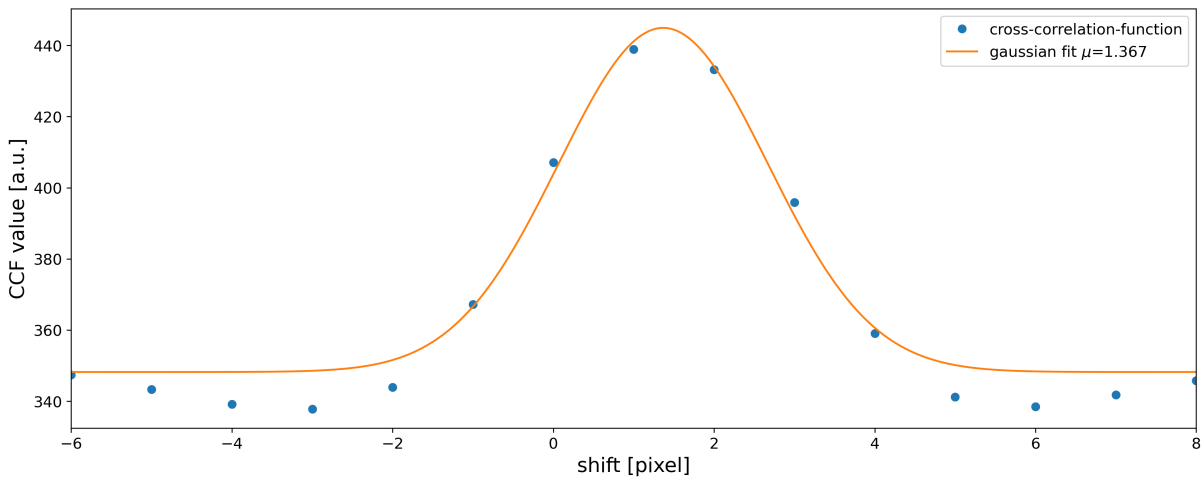

Figure 8: CCF with fitted Gaussian. The maximum of the CCF is at +1 pixel. With the Gaussian, this is corrected to +1.367 pixels.

The order and dispersion direction shifts are then stored together with the filename in a .txt file called "i2_correlation_shifts" in the CERES output folder. Afterwards, the WLS of the good night is shifted by the values found through the I2 correlation to fit the spectra of the "bad" observation night.
This is done in CERES with `create_shifted_wavelength_solution`. As inputs, it takes the shifts in pixel. But as for the WLS creation, the shift in dispersion direction has to be in the amount of redshift z, a conversion has to be done via

$$z = \frac{\text{shift[pixel]} \times k}{\lambda_k} \,. \tag{9}$$

Here, k is the amount of wavelength corresponding to one pixel of the CCD and λ_k is the wavelength at the position where c was taken from. As these values change over the whole CCD, they are determined as a mean of the ten middle pixels and newly calculated for every order. To check that this shift is correct, one can simply compare the I2 spectra as shown in Figure 9. The upper plot shows the original I2 spectrum in orange and the reference in blue. The lower plot shows the shifted I2 spectrum which now aligns well with the reference.
The CCD was changed several times during the survey, hence one needs a separate reference spectrum for each CCD where a bad WLS occurs. Unfortunately, the sensor was swapped shortly before the survey came to an end, and no good ThAr spectra were recorded for this CCD and as the format changed, no other WLS can be applied. As a consequence, the last five nights of observations cannot be analyzed. Reference I2 spectra used were rl20100926_00038 for CCD #6 and rl19990716_00009 for #8. Accordingly, the WLS of nights 20100926 and 19990716 were taken.

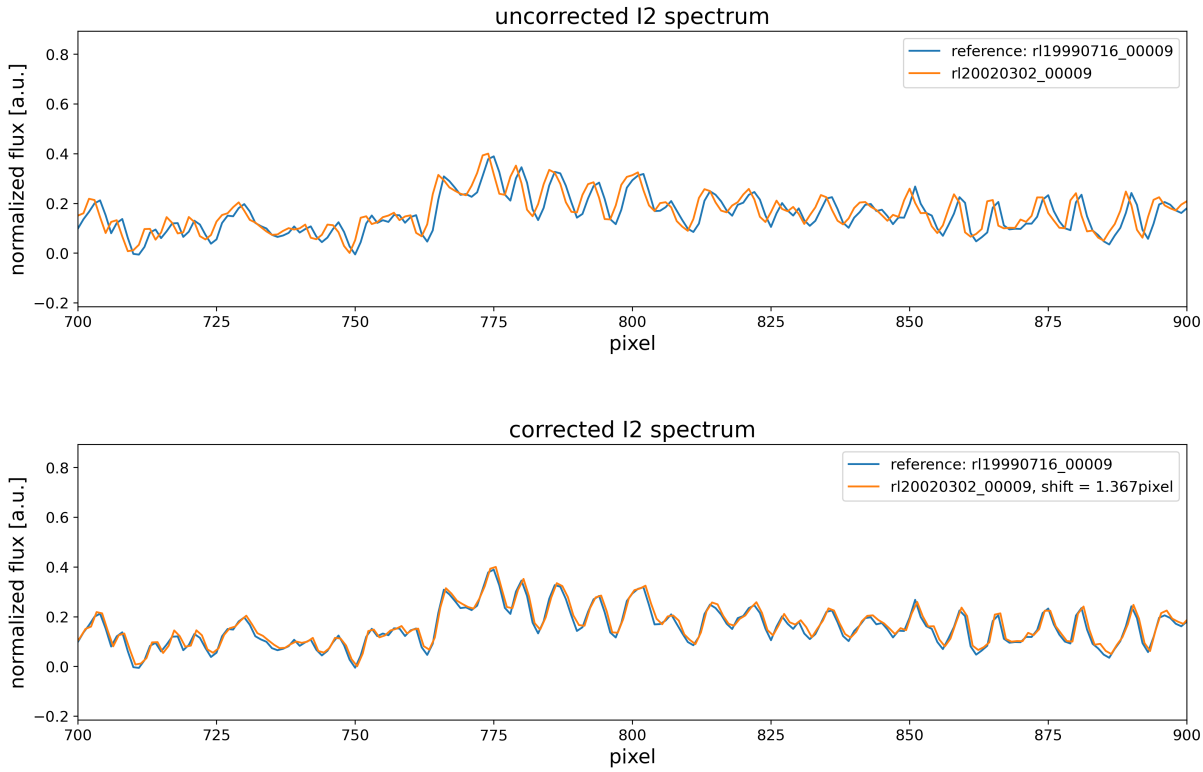

Figure 9: Uncorrected (top) and corrected (bottom) I2 spectra of order 45 from pixel 700 to 900.

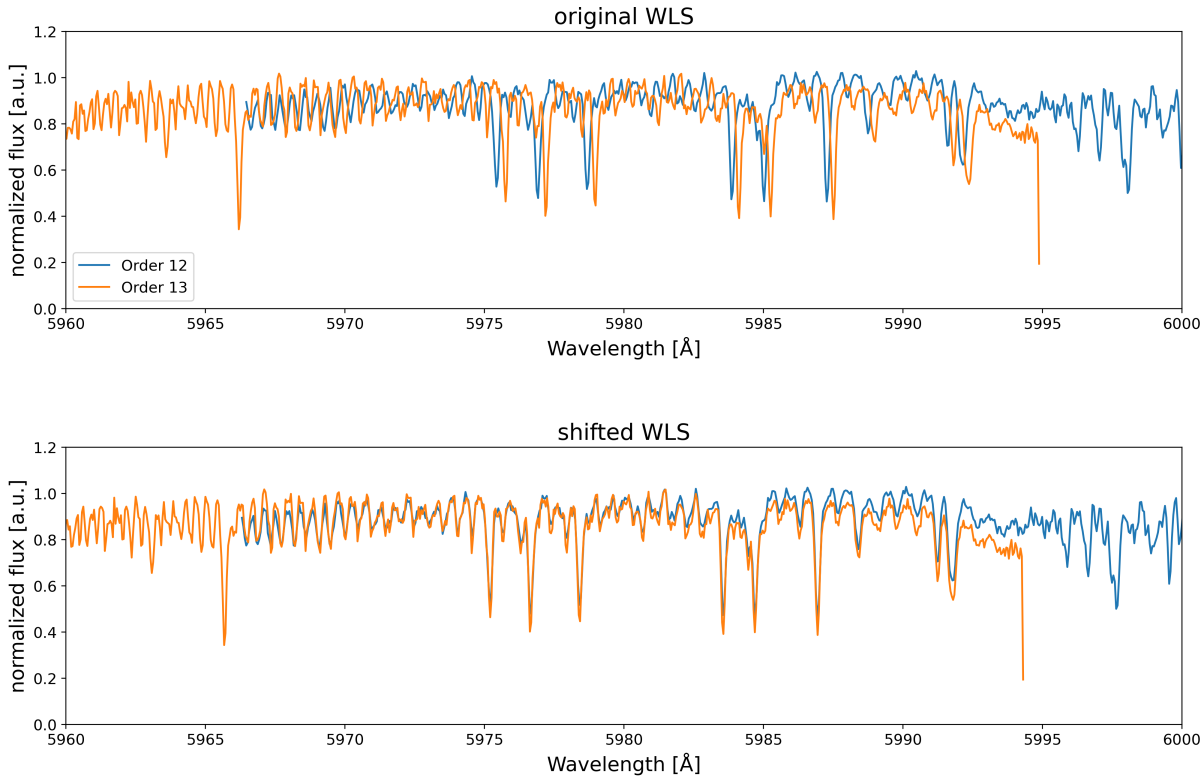

Figure 10: Spectrum of HIP54539. Top: Original WLS, one can clearly see a shift between order 12 and 13. Bottom: Same spectrum but with the new WLS obtained by I2 correlation and shifting the reference WLS. The orders align perfectly. When comparing the original and shifed WLS, one can also see a slight shift to smaller wavelengths of the spectrum.

Figure 10 shows a part of the spectrum from HIP54539 taken on February 19th 2009 with the original WLS in the upper plot. One can clearly see a shift between order 12 and 13. This is due to the bad WLS precision of only $460\,\mathrm{ms}^{-1}$. The plot at the bottom shows the same spectrum, but with the WLS obtained by the I2 correlation and shifting the reference WLS. Now, the well aligned spectral lines are clearly visible.

Theoretically one could replace the ThAr calibration with this I2 calibration method. This would also make it possible to quickly take calibration spectra between the observations during the night as the I2 cell is heated anyways and hence does not need to warm up like the ThAr lamp does. Especially spectrographs that show a large drift over the night like the Waltz would definitely profit from this. But there are also several downsides. First. the I2 spectrum covers only a spectral range from around 5000 to 6300Å whereas the ThAr spans from 4600 up to nearly 8100 Å. This means that we can only assure that the spectrum is well-calibrated in the region where I2 spectral lines are visible. Another but fixable problem is that at the moment, the I2 correlation can not detect any stretching and compression of the spectrum.

6.1.3 Barycentric Velocity

CERES already calculates a rough estimate for the barycentric velocity, as this is needed for the template creation described in section 3.2.1 Create A Deconvolved Stellar Template.
Here, CERES uses an adapted version of the pyodine script for the barycentric correction and is based on `barycorrpy` (Kanodia and Wright 2018). To return the barycentric velocity, one has to input the mid-time of observation, the coordinates of the observatory as well as the star name together with its RA, Dec, PMRA, and PMDec, which are originally obtained from the headers of the FITS files. However, for stars in the Hipparcos catalog, the velocity calculation only uses the HIP number and calculates RA, Dec, PMRA, and PMDec from the catalog parameters. Hence, as for the Lick survey, only stars that are in the Hipparcos catalog are analyzed, one would not need to input the stellar parameters as the HIP number would be sufficient to provide all information needed. Unfortunately, as the Waltz DRS is not only designed for the Lick survey, it also needs to provide a solution for non-HIP stars, for which `bc_CERES.py` insists on inputs for RA, Dec, PMRA, and PMDec.
Again for the Lick Data, the entries in the header of the FITS files are not reliable and sometimes even missing. Hirschbeck (2022) reports about implementing a function to CERES which queries the proper motions of stars from SIMBAD [7]. But as SIMBAD is updated with new values from time to time, it is not consistent to always query the parameters from the website. One solution would be to query the information once and save them in a file to be accessible later. Given the fact that `barycorrpy` offers the option to obtain the parameters from the Hipparcos catalog, the decision was made to use this as it is the most consistent way. Hence, I removed the `query_proper_motion_simbad` from Hirschbeck and implemented a new function called `query_coordinates`. As input, it takes the filename and the FITS header and returns the barycentric velocity calculated by `barycorrpy` using the Hipparcos catalog.

[7] SIMBAD Website.

6.2 pyhalpha

`Pyhalpha`, written by Staudt (2020) as part of his bachelor thesis, is a Python 3 package to calculate the Hα index according to Equation 5. It was later implemented into the Waltz DRS by Hirschbeck 2022. The calculation process can be split up into 3 steps. First, the spectra are wavelength-shifted in such a way that the Hα line is at the exact laboratory wavelength of 6562.808Å. This is done by using the RV calculated by pyodine. Secondly, the integration over the spectral line and the designated continuum windows is performed. Lastly, the error is estimated in a Monte Carlo simulation.
For that, Hirschbeck (2022) developed a pipeline. Due to the fact that at that time, no proper WLS for all spectra was available, she extracted the Hα line orders of the spectra and stored the flux and wavelength in a .csv table. As now, a sufficient WLS for every night is accessible, I removed the part of the pipeline where all the needed spectra and RVs are collected and stored. Besides that, I restructured the pipeline in a way that now all the input and the output paths are defined in the `config_Halpha.py` file and the pipeline only needs the HIP number of the star as input.

6.3 Run Lick Data

All Python 3 scripts used for the analysis of this work can be found in the folder "Run Lick Data" under the git branch "Lick-Data" of the Waltz DRS:

`lick_reduce`	Load the raw files, run through all directories and calculate a WLS for every ThAr spectra found. Filter for the WLS with the best precision in the night and save it.
`lick_correlate_i2s`	Correlate the I2 spectra for nights with no sufficient WLS to obtain the shift values and store them in the "i2_correlation_shifts.txt" file.
`lick_create_shifted_wavesol`	Use the shifts from the I2 correlation to create the shifted WLS and save it in the observation date directory.
`lick_apply_wavesol`	Now apply all WLS to the science spectra. If an observation night directory still has no WLS, then apply the one from the night before.
`lick_sort_HIP`	As the output of CERES is grouped by observation nights, now sort the files by the observation target to prepare it for pyodine. Leave out observations without I2 cell, as these are for the templates.
`lick_collect_templates`	Use the "templates.txt", where the name of each template for a star together with the hot star observations is listed, and group the template observation together with the hot star spectra.
`lick_create_templates`	For every star, read in the template as well as the corresponding hot star spectra, set up the logging and error files and input them all into pyodine.
`lick_model_i2`	For every star, now load the template, model all observations and save the chunk velocities.
`lick_weight_and_combine`	Use either the Lick or the SONG weighting algorithm to combine all the individual results to a time series, correct for the barycentric velocity, and save them.
`lick_h_alpha`	Load the velocity result file together with the CERES output for every star, calculate the Hα index for every observation and save the results.

7 Results

For the analysis of the results, I was provided with the original Lick RVs (RV_{orig}). These were computed with a version of the original code from Butler et al. (1996), which has proven to deliver trustworthy results. Pyodine features two weighting algorithms, one based on the iSONG code (Antoci et al. 2013; F. Grundahl et al. 2017) (SONG weighting hereafter) and one based on the code from Butler et al. (1996) which has been used to calculate the original results (Lick weighting hereafter). The SONG weighting takes into account all chunks of a star time series and calculates weights for every chunk, whereas the Lick weighting tries to filter out bad outlier chunks by several criteria. Refer to Heeren (2021) for a full description of these algorithms. As pyodine also has the possibility to use the median and the standard deviation of the chunks as RVs and ΔRVs, this was also tested.

7.1 Errors

To investigate how well the combination of the single chunks worked, one can take a look at the errors of the final RVs. In principle, these are calculated using a simple standard deviation. When taking a first look at Figure 11, it is clearly visible that the errors calculated via the standard deviation are too big and hence outliers have too high of an influence. These outliers will most likely also have a strong impact on the final RVs, therefore one needs to filter out these bad chunks or apply weights to them to reduce their influence.

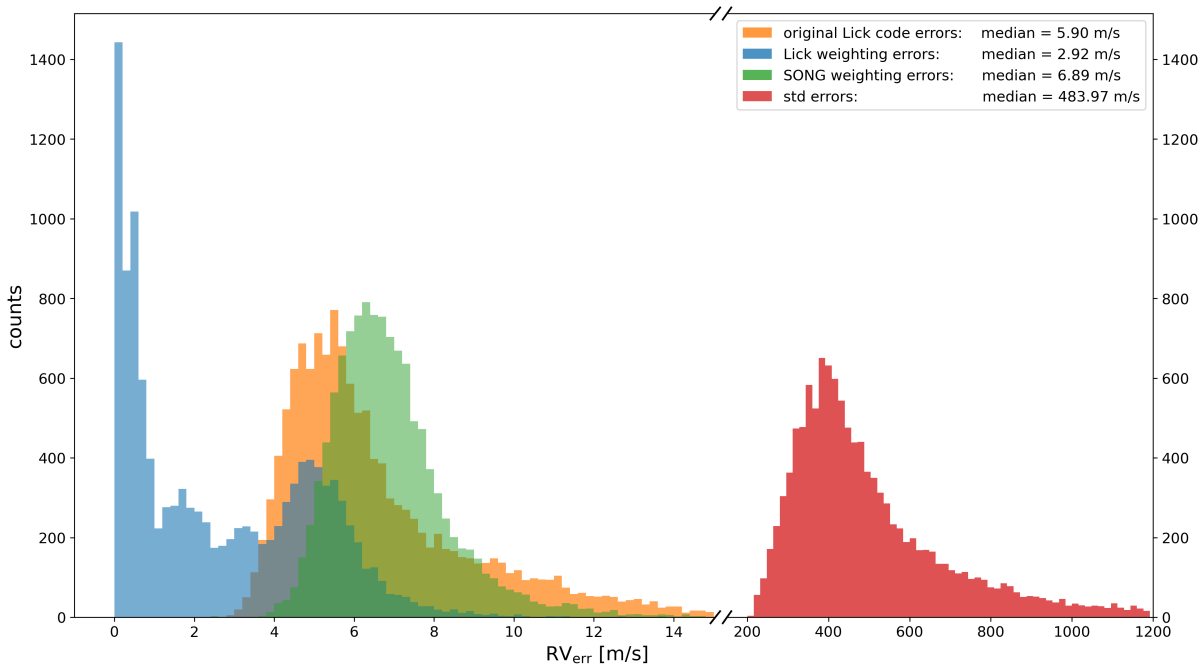

Figure 11: Histogram errors produced by the Lick and SONG weighting algorithms.

Figure 11 shows histograms of the RV errors of all observations, from the three combination methods provided by pyodine, as well as the errors of the original results. The errors from the Lick weighting are underestimated, which is probably due to a too sensitive filtering of outliers. Only the SONG weighting

shows similar results as the original code. In contrast to the original results (94%), the plot shows only around 87% of all errors from the SONG weighting, the other 13% are scattered between $12.5\,\mathrm{ms}^{-1}$ and over $60000\,\mathrm{ms}^{-1}$. The distribution of the SONG errors is a little tighter than the original errors, and the tail towards larger errors is also less pronounced. In Figure 12 top, only the errors from SONG weighting and original RVs errors with value $< 12\,\mathrm{ms}^{-1}$ in both are shown to ensure that nothing went wrong in both the I2 modeling and the weighting and combination process. The upside down histogram at the bottom shows which errors were excluded due to the corresponding error in the other method being $> 12\,\mathrm{ms}^{-1}$. Still, the SONG weighting has errors which are around $1\,\mathrm{ms}^{-1}$ higher on mean. This is also visible in the means of both distributions. For the pyodine-SONG weighting RVs, the mean is $6.8\,\mathrm{ms}^{-1}$, whereas the mean of the original RVs is only slightly smaller at $6.0\,\mathrm{ms}^{-1}$. Another mentionable detail is the tail: When compared to Figure 11, the tail of the original RV distribution decreased. This could be a hint of non-optimal weighting parameters in the SONG algorithm. As for Figure 12, only RV errors that are below $12\,\mathrm{ms}^{-1}$ in the original sample as well as in the pyodine sample are shown. This could could be a hint that the SONG weighting algorithm tries to sort out too many of the chunks.

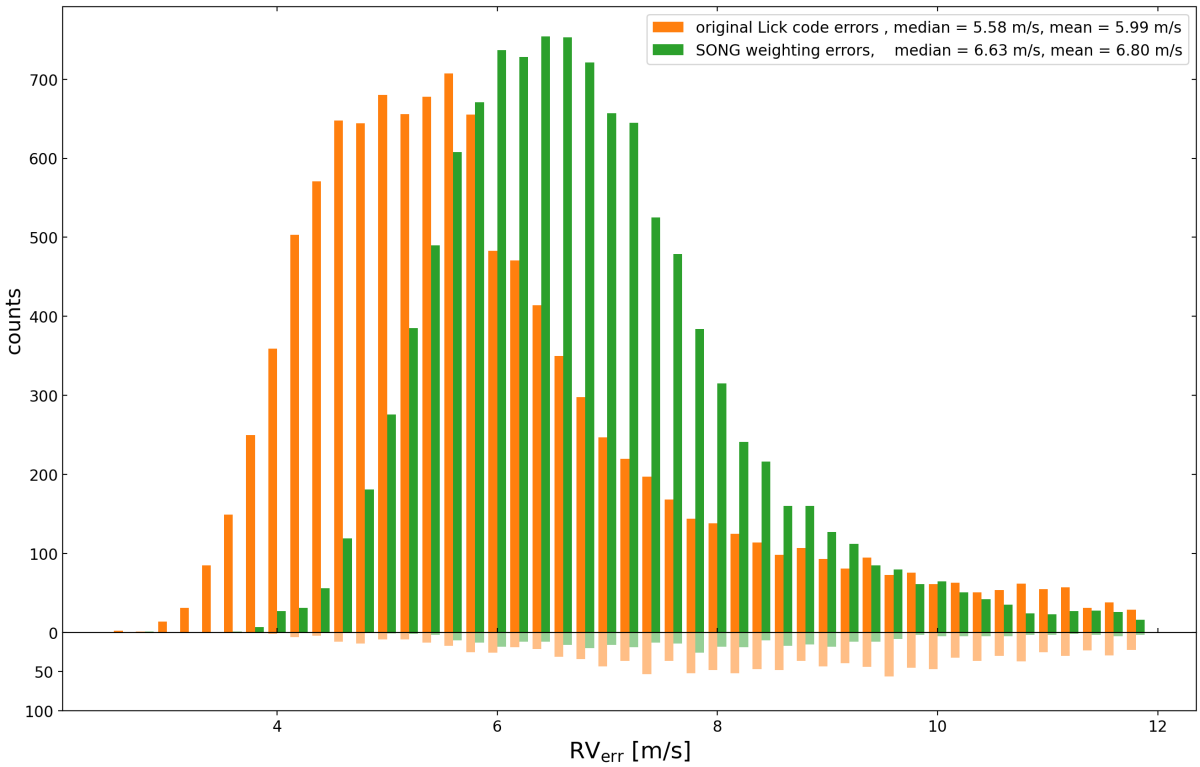

Figure 12: Histogram of the RV errors from the original code and SONG weighting with absolute value $< 12\,\mathrm{ms}^{-1}$. The lower section shows the counts which are excluded due to the fact that the corresponding error in the other sample is $> 12\,\mathrm{ms}^{-1}$

Figure 13 shows a histogram of the percentage of RV errors $< 12\,\mathrm{ms}^{-1}$ per time series of a star. One can see two distinct peaks close to 0 % and close to 100 %. This splits up the sample of stars in two categories and hints that the SONG weighting fails for around 20% of the time series. One reason for that could be binaries where the recorded spectra are a composition of two stars. The Lick sample contains around

20 % binaries which would match the percentage of 100 % errors $> 12\,\mathrm{ms}^{-1}$. One way to determine if a system is a binary is to look at the rms of the measured RVs. For single stars, one would not expect a value of 10 to $1000\,\mathrm{ms}^{-1}$, whereas for binaries, the rms would be huge as the two stars have very different radial velocities. For the calculation of the RV rms, the original Lick RVs were used. The results show that for around 20 % of the stars with 100 % errors $> 12\,\mathrm{ms}^{-1}$ the rms is over $1000\,\mathrm{ms}^{-1}$, but also that around 70 % of the stars have a rms smaller than $30\,\mathrm{ms}^{-1}$. This means that there is a larger percentage of binaries with 100 % errors $> 12\,\mathrm{ms}^{-1}$ but not enough to see a clear correlation. Therefore, 85 time series are left with a rms $> 100\,\mathrm{ms}^{-1}$ and binaries are not causing the high errors.

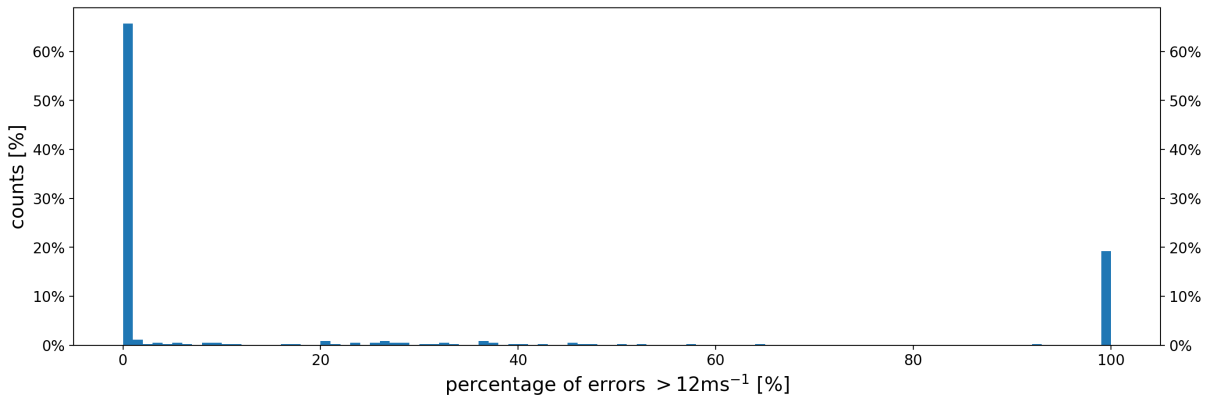

Figure 13: Histogram of percentage of RV errors value $> 12\,\mathrm{ms}^{-1}$ per time series.

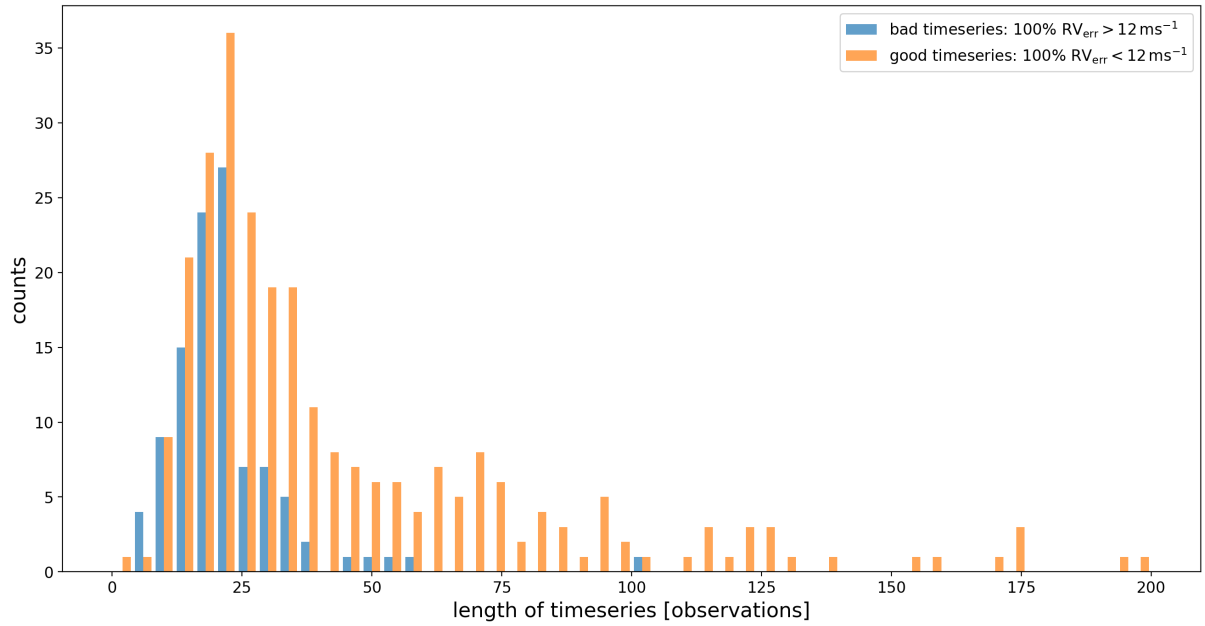

Figure 14: Histogram of the length (in observations) of a time series split up into the two peaks of Figure 13. It seems that it is more likely to get bad errors with fewer obseravtions.

Another reason why the percentage of RV errors $> 12\,\mathrm{ms}^{-1}$ is time series dependent, could be the total number of observations within a given time series. Figure 14 shows the histogram of time series lengths

(in terms of number of observations) split up for stars contained in the two distinct peaks from Figure 13. One can see that the histogram for RV errors with $100\% > 12\,\mathrm{ms}^{-1}$ is centered more at a smaller number of observations per time series and has only one outlier at 100 observations. According to Heeren (2021), this could be an explanation as the SONG weighting is dependent on how many observations a time series has. It could also indicate fainter stars with lower S/N, since the observation time for these is limited to 30 minutes due to the barycentric correction. So, one is in principle not able to achieve a high S/N for these fainter stars and these consequently may have fewer observations because sometimes the weather was not optimal enough to observe them.

This chapter shows that pyodine cannot achieve the same values for the RV errors; neither with the original Lick weighting nor the SONG weighting. Yet, the results look very similar. The Lick weighting seems to filter out too many chunks and underestimates the error whereas the SONG weighting shows errors that are a little bit too high and has 13 % outliers that seem to come only from distinct stars, where all errors are estimated too high.

7.2 Absolute Residuals

Figure 15 shows the absolute residuals ($\Delta RV = RV_{\text{orig}} - RV_{\text{pyodine}}$) between the three weighting methods from pyodine and the original results from -30 to $+30\,\text{ms}^{-1}$. Again, the SONG weighting looks promising and the simple median delivers the worst results. This once more proves the need of a filtering and/or weighting of the single chunk velocities. For the further work, the simple median and std results are not further investigated. In Table 1, the percentages of residuals that fall below a given absolute threshold value are shown. Overall, the distribution follows roughly a normal distribution but the residuals are larger than expected as it is only a difference in software and not in measurement method. One can also see that for the residuals, the weighting method again has a huge impact on the results and that there might be better parameters. From the median and also Table 1 one can also see that there are still a lot of outliers (residuals $> 30\text{ms}^{-1}$), around 25 % for the SONG and nearly 30 % for the Lick weighting

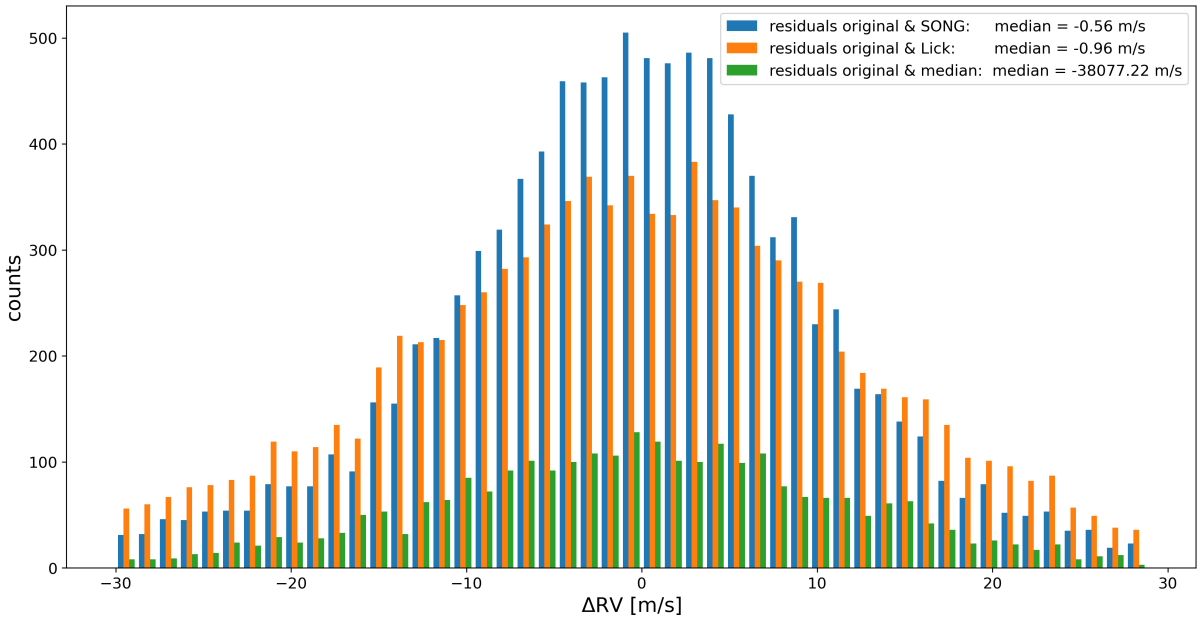

Figure 15: Histogram of the absolute residuals from -30 to $30\,\text{ms}^{-1}$ between the three weighting options and the original RV sample. Outliers with absolute value $> 30\,\text{ms}^{-1}$ are not shown. For the SONG weighting this is around 25 % of all residuals, for the Lick weighting it is at around 30 %.

When comparing the value of RV residuals outlier from SONG weighting (25 %) with the percentage of errors $> 12\,\text{ms}^{-1}$ from SONG weighting 20 % one can think of a possible correlation, however there is no such.

In order to gain a better understanding of how the residuals develop with time, Figure 16 shows histograms of the residuals between the SONG weighting data and the original results in groups of two years. To not be confused by too many colors, the years are grouped into pairs of two. Over time, the median of the distributions shifts to higher values, reaching a maximum of $+2.6\,\text{ms}^{-1}$ for the 2011/2012 histogram, whereas the minimum is at $-2.5\,\text{ms}^{-1}$ in 2001 and 2002. One reason for this shift could be the barycentric velocity correction.

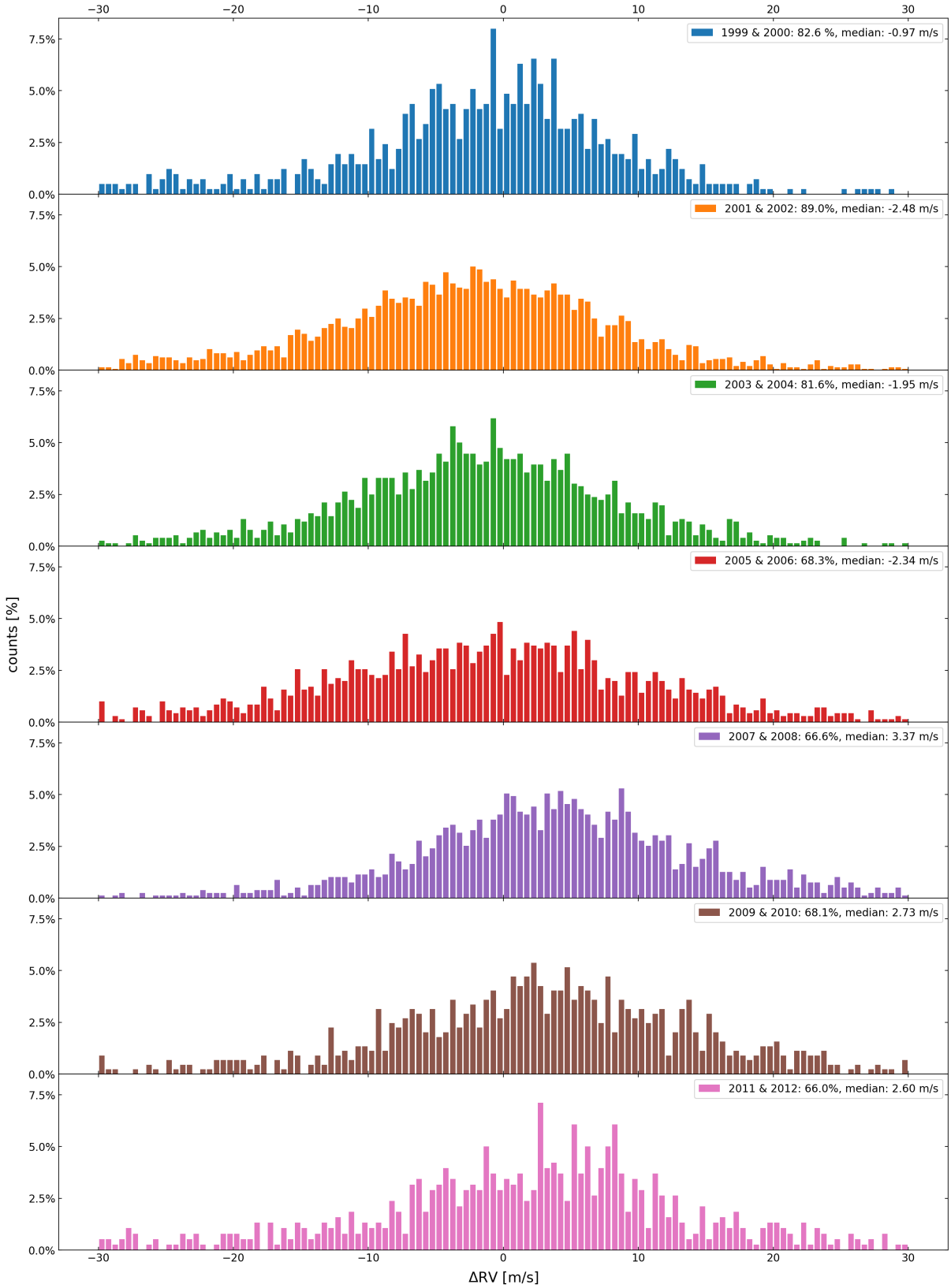

Figure 16: Histogram of the absolute residuals between the SONG weighting and original results. The years are split into groups of two for a better view. Note that the y-axis is given in percent. The value behind the year in the label is the percentage of shown residuals (so $|\Delta RV| < 30\,\mathrm{ms}^{-1}$) from every year.

Table 1: Percentages of absolute residuals under different values for the three weighting algorithms.

$\lvert\Delta RV\rvert$	$< 30\,\mathrm{ms}^{-1}$	$< 10\,\mathrm{ms}^{-1}$ ms^{-1}	$< < 5\,\mathrm{ms}^{-1}$	$< 2\,\mathrm{ms}^{-1}$	$< 1\,\mathrm{ms}^{-1}$
SONG	76.0	52.0	30.1	12.4	6.3
Lick	71.5	41.0	22.5	8.9	4.5
median	19.7	12.1	6.7	2.8	1.6

The RV residuals presented in this chapter show a larger scatter than one would suggest as the RVs are calculated from the same spectra. This would be up to 1 or $2\,\mathrm{ms}^{-1}$ whereas the residuals in this regime make up only 6 and 12 % for SONG weighting and 4.5 and 9 % for Lick weighting. However, since there are differences in these percentages between the two weighting methods, it may well be that these are not yet optimally adapted to the data set. Especially since the Lick weighting, which depends heavily on the filter parameters, also has clear irregularities in the errors.

7.3 Barycentric Correction

The difference in the RVs calculated by pyodine lies not only in the I2 analysis, but also in the calculation of the barycentric velocity (BCV) correction. For the original Lick RVs, the velocities used for the barycentric correction are calculated with a code from McCarthy (1995). Whereas pyodine uses `barycorrpy` (Wright and Eastman 2014) to correct for barycentric velocities up to 1cms^{-1}. In order to get a view on the variation between the BCVs and to determine if it has an influence on the residuals, Figure 17 shows the histogram of the differences between the two versions. As the barycentric correction has a negative sign, it is added to the final RVs. Hence, to obtain the same difference as with the residuals, one has to subtract the `barycorrpy` BCV from the original ones in the .ascii file.

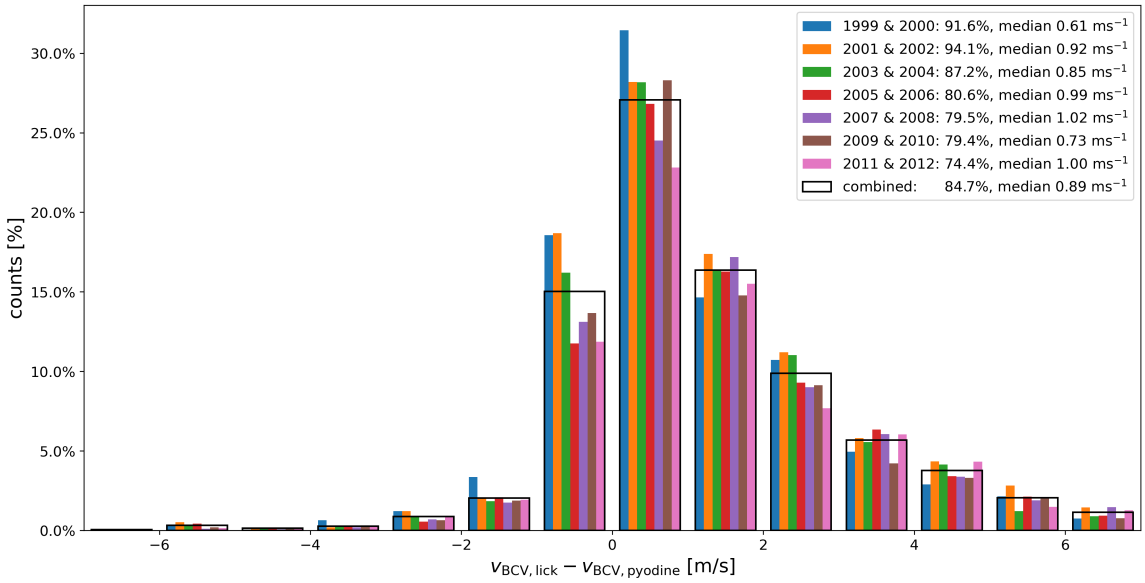

Figure 17: Histogram of the differences in barycentric correction from the old Lick code and pyodine. Around 15% of them are bigger than 7ms^{-1}. The median is at 0.89ms^{-1} and the mean is 1.5ms^{-1}. The colors show the differences by years.

As can be seen by eye, the distribution is shifted to the right and also has a tail to the right. This is also supported by the median ($0.89\,\text{ms}^{-1}$) and the mean ($1.5\,\text{ms}^{-1}$). When only looking at the combined plot, one could think that the tail might be time dependent, so that in the first years, it is smaller and then grows with time. Hence it could be a reason for the trend in the RV residuals. But surprisingly, the tail is somewhat constant through the years, which means that there is some other, not time related systematic behind the absolutely larger RV residuals at later years. Another irregularity is the percentage of residuals shown contained within the x-axis limits of the plot. This is indicated by the percentage values behind the years in the legend of Figure 17. As one can see, it is decreasing from a maximum of 94.1 % down to only 74.7 % in 2011 and 2012. Lastly, I compared the residuals of the final RVs from pyodine with the original Lick RVs where the BCV correction is once done with `barycorrpy` and once with the BCV taken from the original Lick code. The residuals are shown in Figure 18. From the medians, it can already be seen that RVs with original BCVs are slightly more centered towards 0. Additionally, one can also see by eye that the percentage of counts is slightly higher, but not significantly, increased for the original BCVs.

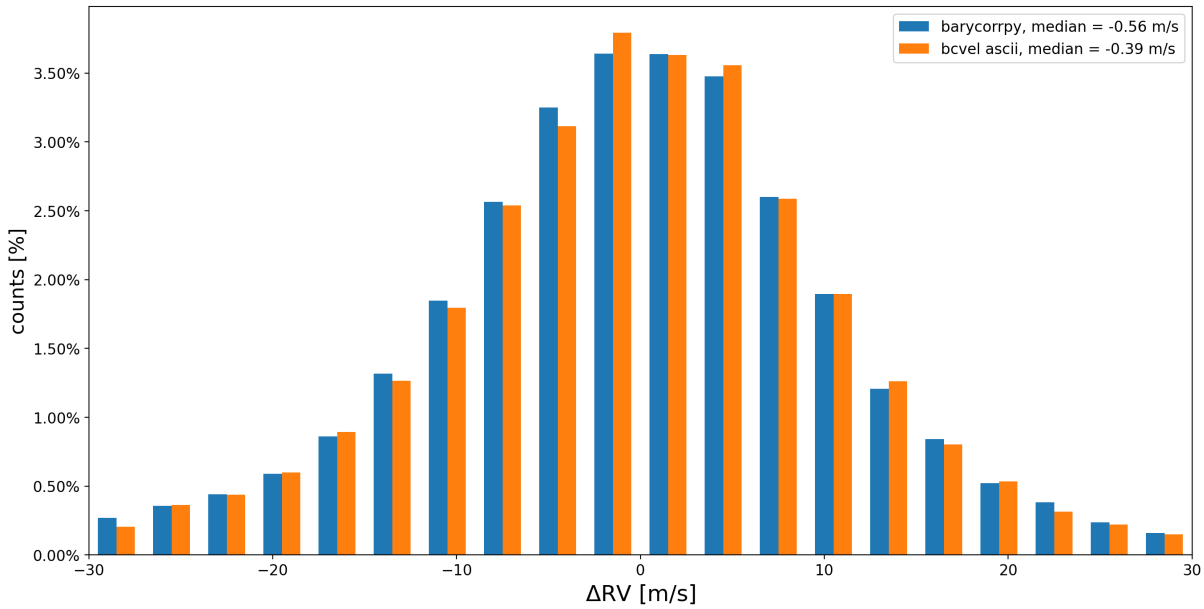

Figure 18: Histogram of RV residuals from pyodine. The blue bars are the ones corrected with `barycorrpy`, for the orange ones the BC velocity was taken from the bcvel.ascii file.

The RV residuals presented in the last chapter suggested a time-dependent systematic. Therefore it was logical to compare the barycentric corrections since they were calculated with different algorithms and parameters. It turned out that the differences in the barycentric corrections are larger than expected, but cannot explain the observed residuals between the RVs of original Lick RVs and SONG weighting with pyodine. In the future, however, the barycentric correction should be investigated further, as the differences should not be larger than 1m/s.

7.4 Relative Residuals

Also for relative residuals

$$\sigma = \frac{RV_1 - RV_2}{\sqrt{\Delta RV_1^2 + \Delta RV_2^2}} \tag{10}$$

the SONG weighting shows a better performance than the Lick weighting. The distribution of relative residuals for SONG and Lick weighting is plotted in Figure 19. For both, a normal distribution is fitted and the FWHM is calculated. Table 2 shows the percentages of RVs contained within different upper and lower limits in terms of σ. For the SONG weighting, around 75 % of all RVs are within $3\,\sigma$ to the original ones from the Lick pipeline.

Table 2: Percentages of relative residuals under different σ values for the Lick and SONG weighting algorithms.

$\lvert res \rvert$	$< 10\ \sigma$	$< 5\sigma$	$< 3\ \sigma$	$< 2\ \sigma$	$< 1\ \sigma$
SONG	86.5	84.0	73.7	73.7	50.2
Lick	60.0	46.1	28.7	28.7	15.4

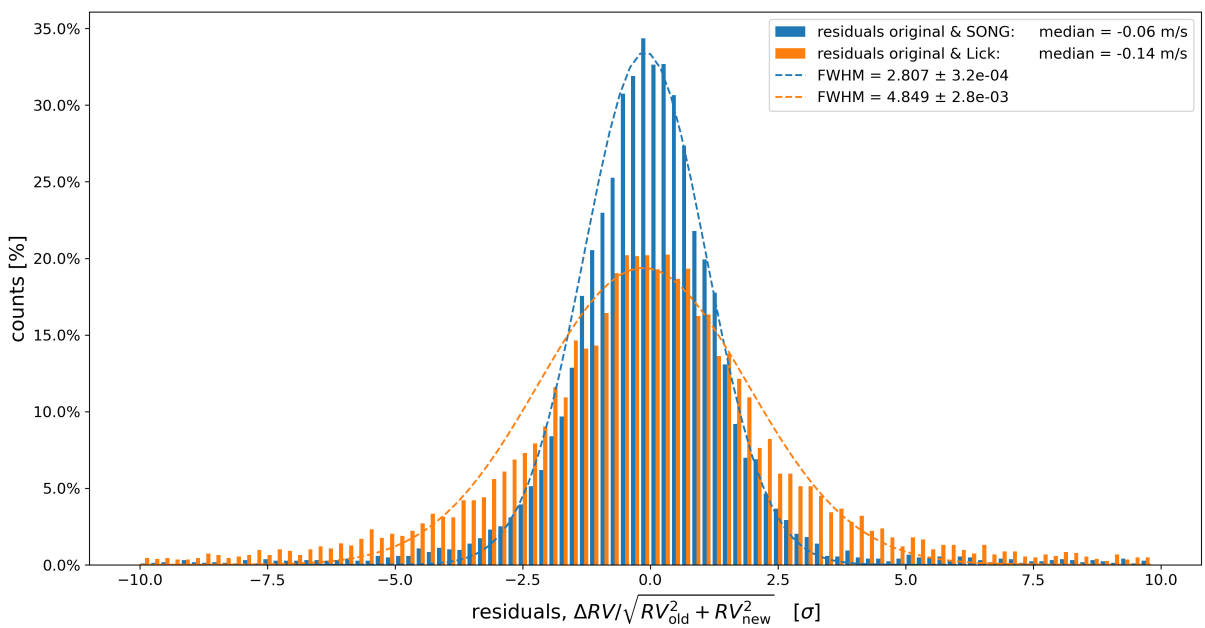

Figure 19: Histogram of the relative residuals between the SONG, Lick weighting and original results. For the SONG weighting, a normal distribution is fitted. The Lick weighting shows a clear offset to the left.

The relative residuals clearly point out that the SONG weighting has overall a good performance with 84 % of RVs are within a 5σ region. The Lick weighting shows a worse performance than for the absolute residuals, which is mainly caused by the many too small errors.

7.5 Published Stellar Companions

To date, ten stars of the Lick survey have published substellar companions. Figure 20 shows the pyodine SONG weighting RV time series (left) of Pollux (HIP37826) and the corresponding generalized Lomb-Scargle (GLS) periodograms (right) (Zechmeister and Kürster 2009). Reffert et al. (2006) reports a planetary companion with a period of 590 ± 5 days which agrees with the period of 592.5 days from the GLS periodogram within the 1σ region.

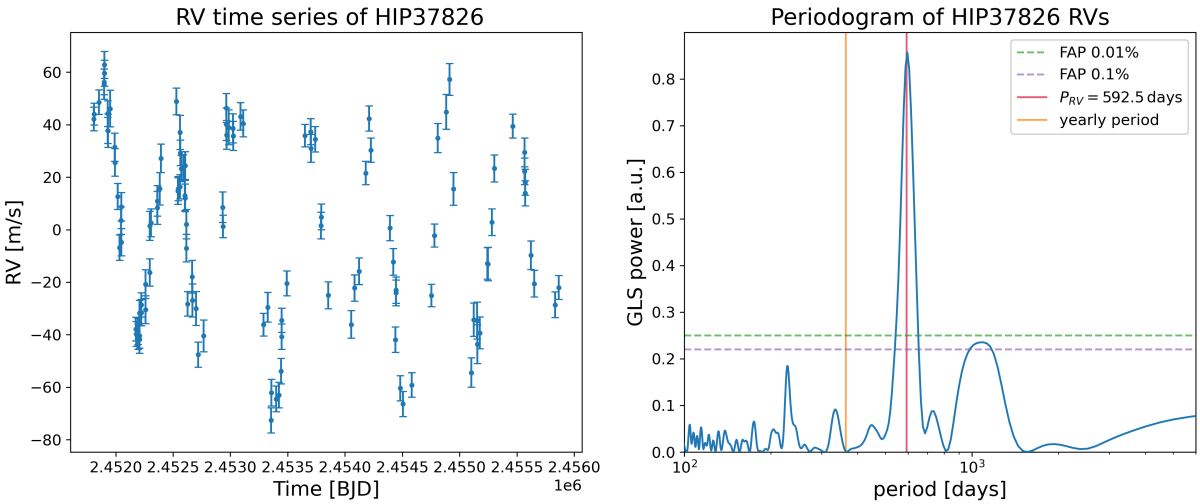

Figure 20: RV time series and periodogram for Pollux (HIP37826).

Table 3: Periods for all stars with published companions in the Lick sample

star	reference	published period [days]	GLS peak [days]	FAP [%]
HIP 5364	Trifonov et al. (2014)	407 ± 3	400.0	$< 10^{-5}$
		740 ± 5	767.4	$< 10^{-5}$
HIP 19011	Pinto et al. (2020)	457.0 ± 1.3	456.9	$< 10^{-5}$
		2273^{+150}_{-116}	1907	8.1×10^{-4}
HIP 31592	Luque et al. (2019)	735	735.9	$< 10^{-5}$
		989	1052.2	9.7×10^{-3}
HIP 34693	Mitchell et al. (2013)	305.5 ± 0.1	305.4	$< 10^{-5}$
HIP 36616	Ortiz et al. (2016)	$299.36^{+0.26}_{-0.31}$	345.4	3.7×10^{-5}
HIP 37826	Reffert et al. (2006)	590 ± 4	592.5	$< 10^{-5}$
HIP 75458	Frink et al. (2002)	536 ± 5	508.3	$< 10^{-5}$
HIP 79540	Pinto et al. (2020)	578 ± 3	577.0	$< 10^{-5}$
HIP 88048	Quirrenbach et al. (2011)	530	530.3	$< 10^{-5}$
		3169	3214.0	$< 10^{-5}$
HIP 114855	Mitchell et al. (2013)	181.4 ± 0.1	181.0	$< 10^{-5}$

For the remaining stars, the RV time series and their periodograms are shown in section 11 Appendix. The calculated periods with their false alarm probability (FAP) as well as the periods given in the reference are shown in Table 3. For some companions, the periods differ more from the reference than others. Reasons for that could either be that for my fits, I used more or fewer data points as the original reference. Another reason might be that some stars (e.g. HIP36616) have eccentric orbits whereas the GLS periodograms only fit for circular orbits. Also, some systems have two or even more companions and the two periods can alter the results from the GLS.

In summary, however, GLS periodograms of SONG weighting pyodine RVs yield results similar to those of the publications. This is satisfactory and shows that the pyodine RVs despite the partly high residuals come to results that align well with the original calculations.

7.6 Hα index

One star that shows stellar activity is HIP5364. Hirschbeck (2022) reports about a peak in the GLS periodogram for the Hα_{ind} at 395 days which would overlap with the RV period of 407 days (399 for a periodogram) found in Trifonov et al. (2014). Figure 21 shows the Hα_{ind} time series of HIP5364 one can already see the period as well as a shift in y direction in the Hα_{ind} between 2.453 and 2.454e6 BJD. This shift is very likely introduced by the CCD change from CCD#6 to CCD#8.

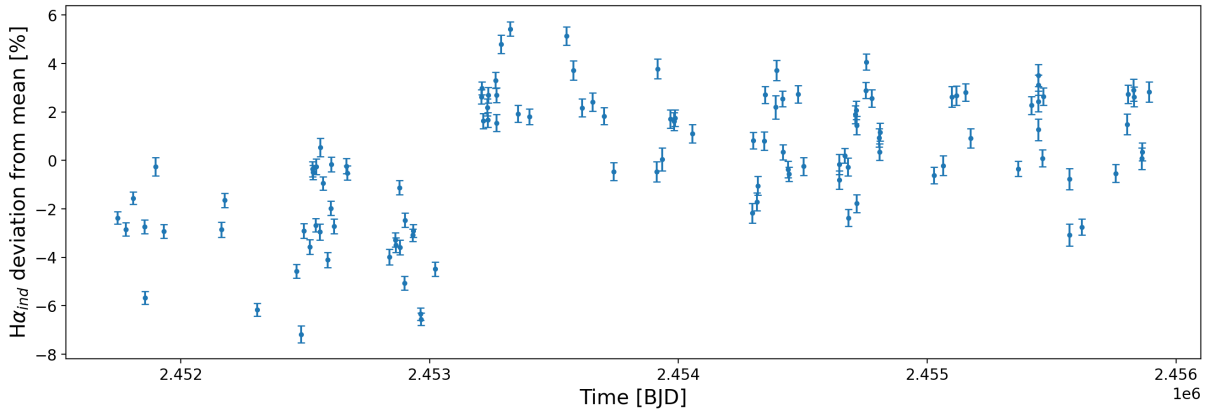

Figure 21: Hα_{ind} time series of HIP5364

The shift can be clearly seen in Figure 22, where all calculated Hα_{ind} for observations of the Lick survey are plotted against the date of observation. They are split into the orange ones where CCD#6 was used and the blue ones where CCD#8 was built in. The linear trends I fitted match the ones found by Hirschbeck (2022).

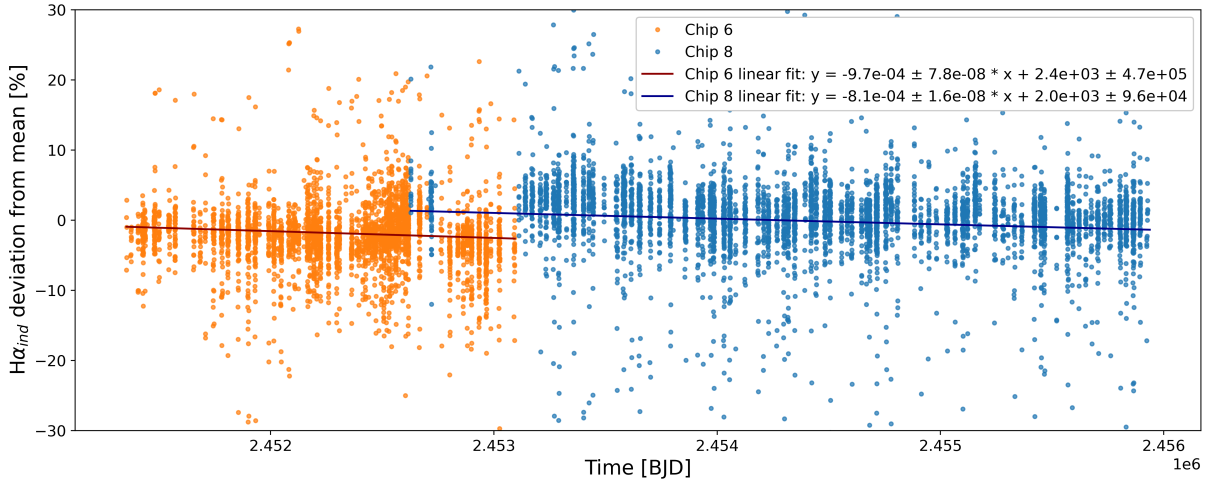

Figure 22: Hα_{ind} for all observations of the Lick survey against their date. The used CCDs are color-coded and for every CCD a linear Trend is fitted.

The RV and the corrected Hα time series together with their periodograms are plotted in Figure 23. For the RV time series, one detects two clear peaks at around 400 and 767 days. This matches the published periods. The periodogram for the Hα_{ind} below shows four peaks. The one on the right can be neglected as this corresponds to the time between the first and last observation. One can also see the peaks at around 1000 days and the two at around 527 and 626 days that are also found by Hirschbeck (2022) and Staudt (2020). The peak at the very left is at 378 days. When looking at Figure 24, one can clearly see how this peak in Hα_{ind} overlaps with the detected peak in the RVs. Hence, this might be a hint that the RVs are introduced by stellar activity. In contrast to only a FAP of 80% by Hirschbeck (2022), I can report a high significance for this peak in the $H\alpha_{ind}$ at nearly down to 0.1% FAP.

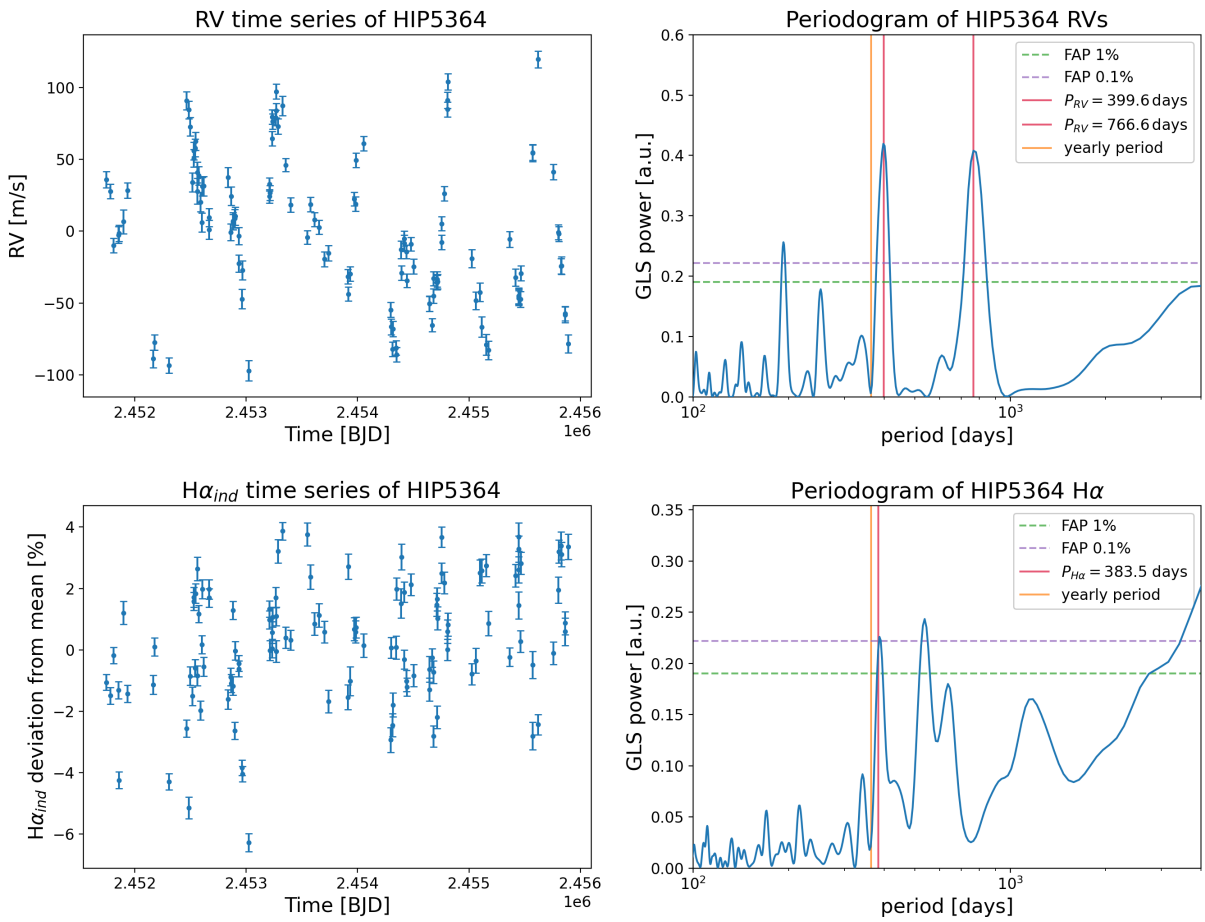

Figure 23: Top: RV time series (right) and corresponding periodogram (left). Bottom Hα_{ind} time series with the periodogram.

One can also see a high peak in the periodogram of the RVs at around 200 days with a FAP of under 0.1% in Figure 24. In contrast to the RVs this peak is not visible in the Hα_{ind} periodogram. The interesting part is that the period of around 200 days would match the the half of the period at 400 days. However if it would be a mode it should be visible in the Hα_{ind} but this could also be not visible due to too high noise. This should definitely be investigated further in the future.

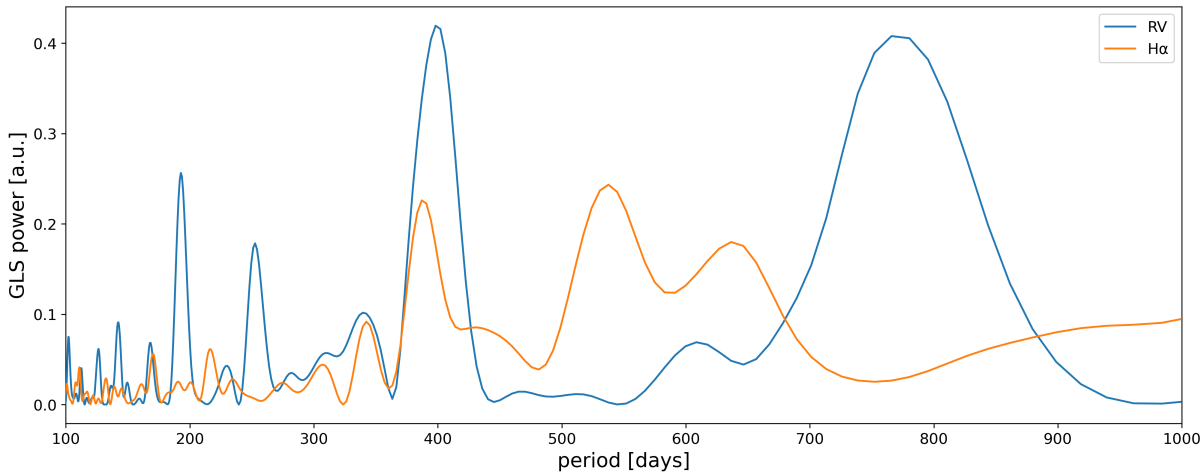

Figure 24: Periodograms for the RV and Hα_{ind} time series of HIP5364. One can clearly see the overlapping peaks at around 390 days.

This chapter shows that new insights arise with the re-computation of the RVs. For HIP5364, this is especially the case in the Hα_{ind} time series, since there are now more data points than in the previous. This results in the peak in the periodogram now having a FAP of less than 0.1 % whereas previously this was 80 % (Hirschbeck 2022) I can also verify the trend in the Hα_{ind} with a offset at the time where the CCD was changed. For the RVs also a new peak in the GLS periodogram is now visible at 200 days with a FAP of around 0.1 %. This should be investigated more in the future to determine weather it is just a mode of the peak at 400 days or an independent period.

7.7 Lick Weighting Algorithm

As visible in Figure 11 the Lick weighting algorithm shows irregularities when computing the RV errors. Butler et al. (1996) shows that the minimal RV error of a spectrum with S/N of around 200 is 3ms^{-1}. The Lick spectra have a S/N of around 100 and hence the achievable precision in RV is around 6ms^{-1} which is also clearly visible in the median of the original RV results of 5.9ms^{-1}. Hence I tried to adapt the parameters for the Lick weighting in order to correct this irregularity. First tests show, that by adjusting the maximum allowed χ^2 (of the chunk model to the observed spectrum) value from the default of 10^8 down to 3×10^5 the RV errors are mostly distributed between 3 and 7ms^{-1}. This is shown in Figure 25. Unfortunately by decreasing the χ^2 value the precision of RVs got worse. They scatter a lot as the residuals show no distribution at all.

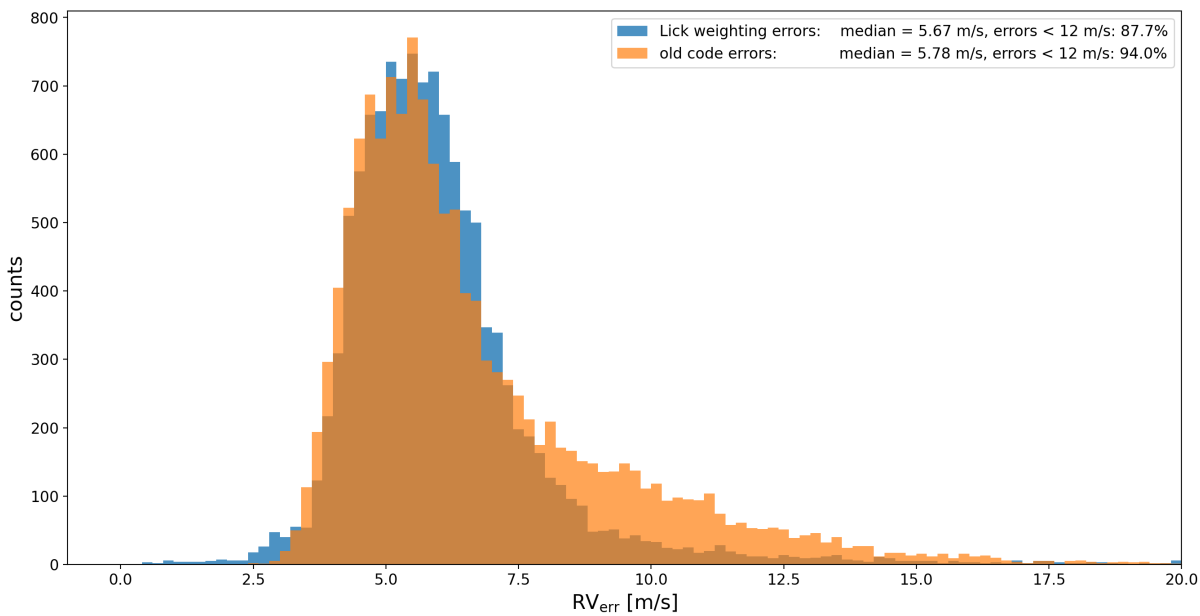

Figure 25: Histogram of RV errors from the Lick weighting with $\chi^2 = 3 \times 10^5$ compared with original results.

This chapter shows that there is definitely room for improvement, especially for the Lick weighting, since this depends very much on the filter parameters. But also the SONG weighting can be improved, especially around the many outlier which occur only for single time series.

8 Conclusion

8.1 Summary

In this work, I analyzed 15.191 spectra of 374 stars taken between 1999 and 2012 with the Hamilton-Echelle spectrograph at Lick Observatory in California. For this re-analysis, the first open flexible iodine reduction software for precise radial velocities, pyodine (Heeren et al. 2023, subm.), was used. I am now able to provide a wavelength calibrated version of these spectra for further investigations. The most challenging part of this was to provide wavelength solutions, even for observation nights with unusable ThAr spectra.

For the calculation of precise radial velocities, pyodine requires spectra with a wavelength calibration as input. Since the original Lick spectra provided to me did not have such, I used the Waltz DRS (Heeren 2021) to apply a wavelength solution (WLS) obtained from ThAr spectra. Hirschbeck (2022) has already shown that this wavelength calibration fails for about 40% of all observing nights. Therefore, I first optimized the algorithms for WLS creation in Waltz DRS. Then, I implemented a function that creates a reference WLS according to shifts determined by correlating iodine Flat spectra. Thus, I was able to provide a good wavelength calibration for each observation night.

In the second part of the thesis, I use pyodine to calculate precise radial velocities and compare them with the original results calculated with the code from Butler et al. (1996), which has proven to deliver trustworthy results. Overall, pyodine seems to deliver good RVs which correspond in large parts with the original results. Nevertheless, there is still room for improvement, especially for the Lick weighting algorithm.

8.2 Discussion and Future Prospects

Starting with the adaptions I made to the Lick files: By adding the needed information to the FITS header of the files, pyodine is now able to detect the used instrument and together with the new introduced mid time from the logsheet, pyodine can calculate precise barycentric velocity corrections. For the files where the coordinates and proper motions of the star were missing, I changed the source for them to the Hipparcos catalog, which ensures consistency of the parameters. However, since this could change in the future with updates of `barycorrpy` to, for example, Gaia data, and since the Hipparcos catalog of course only covers HIP stars, a separate catalog should be created in the future for the stars observed with the Waltz.

Next up are my additions to the Waltz DRS: In the first step I showed that there was a lot of improvement in how the wavelength solution is created by reducing the percentage of bad WLS from 42 % down to 14 %. From my analysis, I think that this is the maximum achievable as the ThAr spectra from 2011 ongoing make up the most of these 14 % and are in a very bad condition as can be seen in Figure 7. The shift of a WLS based on the cross-correlation of iodine spectra is used to provide a proper WLS for these nights. At the moment, only one ThAr/I2 spectrum is used to create a WLS for one night, but in order to improve this even further, one could instead use all available spectra of one night, create a separate WLS of each of them and interpolate between them. This is currently done for the Waltz

telescope as it shows drifts of over 500ms^{-1} in one observation night and over 2500ms^{-1} over the time span of two weeks (Heeren 2021).

As the iodine correlation method seems to work very well, it could in principle replace the ThAr calibration, if one is only interested in the part of the spectrum which is covered by the iodine as it cannot detect shifts beyond that. Nevertheless, the Waltz could profit from this method, as the ThAr spectra during the observation could be replaced with I2 Flats. This would have the advantage of being super fast, as one would only need to quickly switch on the halogen lamp instead of having to wait until the ThAr lamp has heated up.

The next step is the pyhalpha package. For my analysis, I removed the step of saving the order with the Hα spectral line in a separate CSV file and regrouped the whole Hα pipeline. The following step here would be to implement the calculation of the Hα_{ind} directly into the last part of pyodine where the weighting and combining of the chunks is done and to add the Hα_{ind} as well as the error ΔHα_{ind} to the results object to be easily accessible.

The final RV results from pyodine appear to be consistent with the original results, although they are not exactly the same. For the SONG weighting, this is not very surprising as it uses all chunks of a time series and applies weights to them whereas the original algorithm tries to filter out bad chunks and then just takes the simple median. For the Lick weighting, there seems to be some sort of systematic, especially in the errors. Figure 11 shows two peaks and the right peak seems to align well with the original results. Hence, I tried to adapt the weighting parameters in section 7.7 Lick Weighting Algorithm, which caused the errors to follow the original distribution in Figure 25 but also lead to extremely bad RV residuals. One irregularity that I encountered while investigating this is that in the code, the filtering is for bad χ^2 values whereas Heeren (2021) describes the filtering for χ^2_{red} like it is in the original code from Butler et al. (1996). This might be a hint that the Lick weighting is not completely the same as in the original code and definitely should be investigated further in the future. The SONG weighting should also be examined more closely as there seem to be 25 % outliers in residuals and 13 % outliers in errors that are not correlated and whose origins are not known.

Although there are differences in the barycentric correction between the original results and the ones calculated by pyodine, these differences seem to be marginal and have no real influence on the final RVs. For the future, as said before, one should introduce a new catalog for Waltz stars to be independent of updates and the catalog used in `barycorrpy`.

The periodograms for stars with published companions work well and all show acceptable results with FAP values below 10^{-5} for most of the periods. For the future, this now allows for a re-analysis of the RV results for these stars which might lead to other results that could reveal new astrophysical insights wherever systematic differences occur as already shown for HIP36616 by Heeren (2021).

9 Acknowledgments

Finally, I would like to thank all the people who supported me during this bachelor thesis. First and foremost Dr. Paul Heeren, who answered all my questions about the Waltz DRS at all times. Thank you for being my suffering partner when it comes to the many quirks of the Lick data set and proofreading my thesis. I am thanking Dane Späth for answering all my astronomy related questions and for proofreading my thesis. I would also like to thank the entire LSW exoplanet group for all the helpful tips and for everything I have learned in the last half year. I am also very grateful for being part of the Waltz telescope project during my time at LSW and for the observation nights I was able to spend at the Waltz telescope. Special thanks to P.D. Dr. Sabine Reffert for being my supervisor for this thesis and giving me guidance when needed. I also want to thank my parents for the support during the last 22 years and for teaching me to follow my heart. Lastly, I want to thank Sophie for riding this rollercoaster with me. Without you, your love and your support, time wouldn't be as enjoyable. I can't wait to see what the future holds for us.

"Remember to look up at the stars and not down at your feet. Try to make sense of what you see and wonder about what makes the universe exist. Be curious. And however difficult life may seem, there is always something you can do and succeed at. It matters that you don't just give up."

Stephen Hawking

10 References

Andersen, M. F. et al. (2014). "Hardware and software for a robotic network of telescopes - SONG". In: *Revista Mexicana de Astronomia y Astrofisica Serie de Conferencias* 45. DOI: https://arxiv.org/abs/1901.08300.

Antoci, V. et al. (2013). "Searching for solar-like oscillations in the δ Scuti star ρ Puppis". In: *Monthly Notices of the Royal Astronomical Society* 435.2, pp. 1563–1575. DOI: https://doi.org/10.1093\%2Fmnras\%2Fstt1397.

Boisse, I. et al. (2009). "Stellar activity of planetary host star HD 189 733". In: *Astronomy & Astrophysics* 495.3, pp. 959–966. DOI: https://doi.org/10.1051\%2F0004-6361\%3A200810648.

Brahm, Rafael et al. (2017). "CERES: A Set of Automated Routines for Echelle Spectra". In: *Publications of the Astronomical Society of the Pacific* 129.973, p. 034002. DOI: https://dx.doi.org/10.1088/1538-3873/aa5455.

Butler, R. Paul et al. (1996). "Attaining Doppler Precision of 3m s-1." In: DOI: https://doi.org/10.1086/133755.

Eversberg, Thomas and Klaus Vollmann (2015). *Spectroscopic Instrumentation*. Springer Berlin, Heidelberg. DOI: https://doi.org/10.1007/978-3-662-44535-8. URL: https://link.springer.com/book/10.1007/978-3-662-44535-8.

Fischer, D. A. et al. (2014). "Exoplanet Detection Techniques". In: *Protostars and Planets VI*. University of Arizona Press. DOI: https://doi.org/10.2458\%2Fazu_uapress_9780816531240-ch031.

Frink, Sabine et al. (2002). "Discovery of a Substellar Companion to the K2 III Giant ι Draconis". In: *The Astrophysical Journal* 576.1, p. 478. DOI: https://dx.doi.org/10.1086/341629.

Frink, Sabine et al. (2001). "A Strategy for Identifying the Grid Stars for the Space Interferometry Mission". In: *Publications of the Astronomical Society of the Pacific* 113.780, p. 173. DOI: https://dx.doi.org/10.1086/318610.

Grundahl, F. et al. (2017). In: 836.1, p. 142. DOI: https://dx.doi.org/10.3847/1538-4357/836/1/142.

Grundahl, Franck et al. (2008). "Stellar Oscillations Network Group – SONG". In: *Journal of Physics: Conference Series* 118, p. 012041. DOI: https://doi.org/10.1088\%2F1742-6596\%2F118\%2F1\%2F012041.

Heeren, Paul (2021). "Testing Planet Candidates around Giant Stars: Computation and Analysis of High Precision Radial Velocities." DOI: https://doi.org/10.11588/heidok.00030357.

Heeren, Paul et al. (2023). "Pyodine: An open, flexible iodine reduction software for precise radial velocities." Version subm. In.

Hirschbeck, Franziska M. (2022). "Analysis of the Hα Index for G and K Giant Stars in the Framework of the Waltz Telescope Project". Landessternwarte, Department of Physics and Astronomy, Heidelberg University.

Horne, K. (1986). "AN OPTIMAL EXTRACTION ALGORITHM FOR CCD SPECTROSCOPY." In: *Publications of the Astronomical Society of the Pacific* 98.604, p. 609. DOI: https://dx.doi.org/10.1086/131801.

Kanodia, Shubham and Jason Wright (2018). "Python Leap Second Management and Implementation of Precise Barycentric Correction (barycorrpy)". In: *Research Notes of the AAS* 2.1, p. 4. DOI: https://dx.doi.org/10.3847/2515-5172/aaa4b7.

Luque, R. et al. (2019). "Precise radial velocities of giant stars - XIII. A second Jupiter orbiting in 4:3 resonance in the 7 CMa system". In: *A&A* 631, A136. DOI: https://doi.org/10.1051/0004-6361/201936464.

Marcy, Geoffrey W. and R. Paul Butler (1992). "PRECISION RADIAL VELOCITIES WITH AN IODINE ABSORPTION CELL". In: *Publications of the Astronomical Society of the Pacific* 104.674, p. 270. DOI: https://dx.doi.org/10.1086/132989.

Marsh, T. R. (1989). "THE EXTRACTION OF HIGHLY DISTORTED SPECTRA". In: *Publications of the Astronomical Society of the Pacific* 101.645, p. 1032. DOI: https://dx.doi.org/10.1086/132570.

Mayor, M et al. (2003). "Setting New Standards with HARPS". In: *The Messenger* 114, p. 20. URL: http://www.eso.org/sci/publications/messenger/archive/no.114-dec03/messenger-no114-20-24.pdf.

McCarthy, Chris (1995). "Transformation of Doppler shifts to the solar system barycenter". San Francisco State University.

Mitchell, David S. et al. (2013). "Precise radial velocities of giant stars - V. A brown dwarf and a planet orbiting the K giant stars minorum and 91 Aquarii". In: *A&A* 555, A87. DOI: 10.1051/0004-6361/201321714. URL: https://doi.org/10.1051/0004-6361/201321714.

Ortiz, Mauricio et al. (2016). "Precise radial velocities of giant stars - IX. HD 59686 Ab: a massive circumstellar planet orbiting a giant star in a 13.6 au eccentric binary system". In: *A&A* 595, A55. DOI: https://doi.org/10.1051/0004-6361/201628791.

Pinto, Marcelo Tala et al. (2020). "Precise radial velocities of giant stars - XIV. Evidence of planetary companions around HD 25723, 17 Sco, 3 Cnc, and 44 UMa". In: *A&A* 644, A1. DOI: https://doi.org/10.1051/0004-6361/202038285.

Quintana, Elisa V. et al. (2014). "An Earth-Sized Planet in the Habitable Zone of a Cool Star". In: *Science* 344.6181, pp. 277–280. DOI: 10.1126/science.1249403.

Quirrenbach, Andreas et al. (2011). "Planets around Giant Stars". In: 1331. DOI: 10.1063/1.3556189.

Rasmussen, René Tronsgaard (2016). "Precise measurements of stellar radial velocities. A new, open-source pipeline for iodine cell Doppler spectroscopy." Department of Physics and Astronomy, Aarhus University.

Reffert, Sabine et al. (2006). "Precise Radial Velocities of Giant Stars. II. Pollux and Its Planetary Companion". In: *The Astrophysical Journal* 652.1, p. 661. DOI: https://dx.doi.org/10.1086/507516.

Saio, Hideyuki et al. (2015). *Oscillatory convective modes in red giants: a possible explanation of the long secondary periods*. DOI: https://doi.org/10.1093/mnras/stv1587.

Shen, Meng et al. (2018). "New spectral reduction algorithm for echelle spectrometer in laser-induced breakdown spectroscopy". In: *Opt. Express* 26.26, pp. 34131–34141. DOI: 10.1364/OE.26.034131. URL: https://opg.optica.org/oe/abstract.cfm?URI=oe-26-26-34131.

Staudt, Patrick (2020). "H ALPHA VARIATIONS OF G AND K GIANTS". Landessternwarte, Department of Physics and Astronomy, Heidelberg University.

Struve, Otto (1952). "roposal for a project of high-precision stellar radial velocity work". In: *The Observatory* 72, pp. 199–200. URL: https://ui.adsabs.harvard.edu/abs/1952Obs....72..199S/abstract.

Trifonov, Trifon et al. (2014). "Precise radial velocities of giant stars - VI. A possible 2:1 resonant planet pair around the K giant star η Ceti". In: *A&A* 568, A64. DOI: https://doi.org/10.1051/0004-6361/201322885.

Wolszczan, A. and D. A. Frail (1992). "A planetary system around the millisecond pulsar PSR1257 + 12". In: *Nature* 355.6356, pp. 145–147. ISSN: 1476-4687. DOI: https://doi.org/10.1038/355145a0.

Wolthoff, Vera et al. (2022). "Precise radial velocities of giant stars - XVI. Planet occurrence rates from the combined analysis of the Lick, EXPRESS, and PPPS giant star surveys". In: *A&A* 661, A63. DOI: https://doi.org/10.1051/0004-6361/202142501.

Wright, Jason and J. Eastman (2014). "Barycentric Corrections at 1 cm s-1 for Precise Doppler Velocities". In: *Publications of the Astronomical Society of the Pacific* 126.943, p. 838. DOI: https://dx.doi.org/10.1086/678541.

Zechmeister, M. and M. Kürster (2009). "The generalised Lomb-Scargle periodogram - A new formalism for the floating-mean and Keplerian periodograms". In: *A&A* 496.2, pp. 577–584. DOI: https://doi.org/10.1051/0004-6361:200811296.

Weblinks

1 NASA Exoplanet Archive: https://exoplanetarchive.ipac.caltech.edu/cgi-bin/TblView/nph-tblView?app=ExoTbls&config=PSCompPars (last 30.01.2023).

2 LSW Exoplanets: https://www.lsw.uni-heidelberg.de/projects/exoplanets/ (last 30.01.2023).

3 NASA Exoplanet Archive: https://exoplanetarchive.ipac.caltech.edu/exoplanetplots/ (last 30.01.2023).

7 SIMBAD Website: https://simbad.u-strasbg.fr/simbad/sim-fid (last 30.01.2023).

11 Appendix

RV Periodograms with a range from 10^2 to 10^4 days

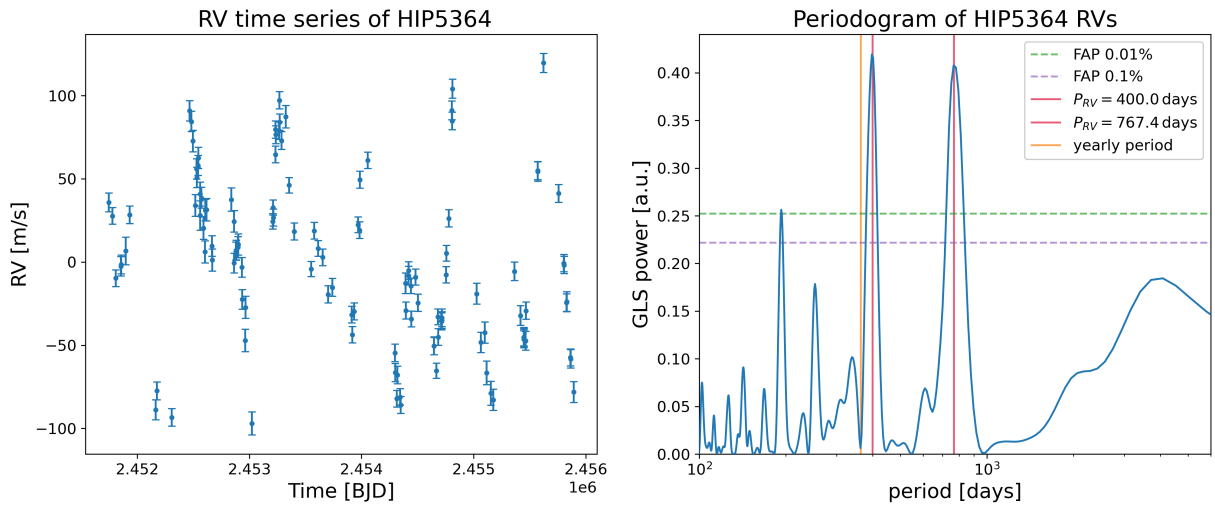

Figure 26: Periodograms for the RV time series of HIP5364.

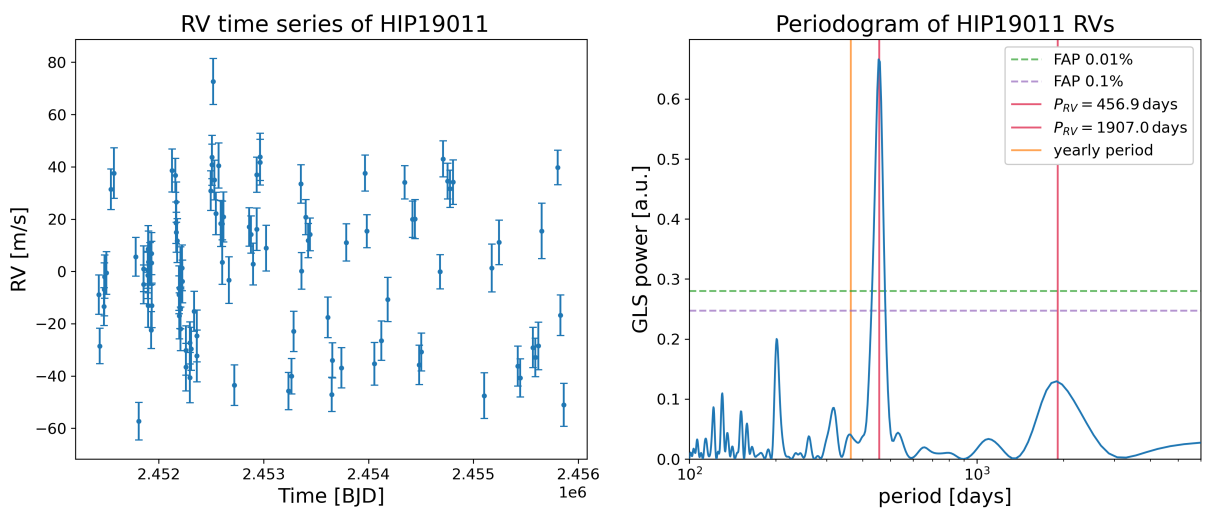

Figure 27: Periodograms for the RV time series of HIP19011.

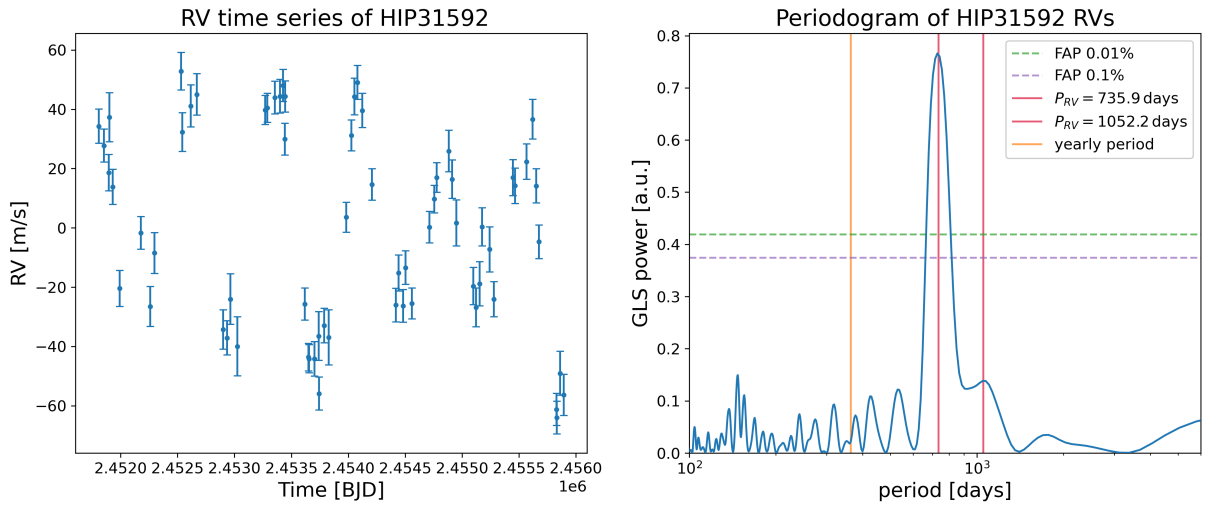

Figure 28: Periodograms for the RV time series of HIP31592.

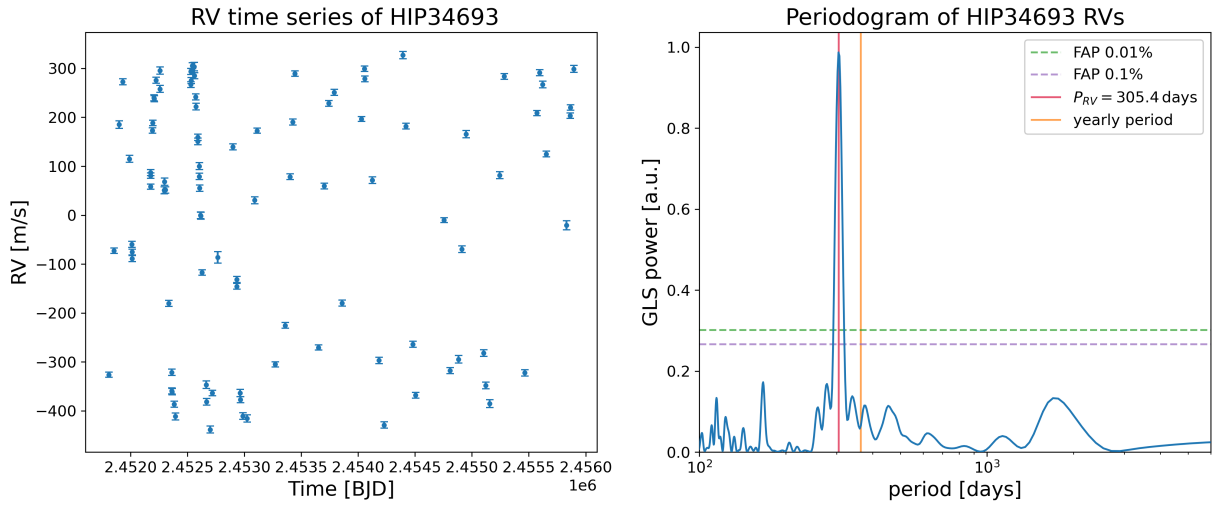

Figure 29: Periodograms for the RV time series of HIP34693.

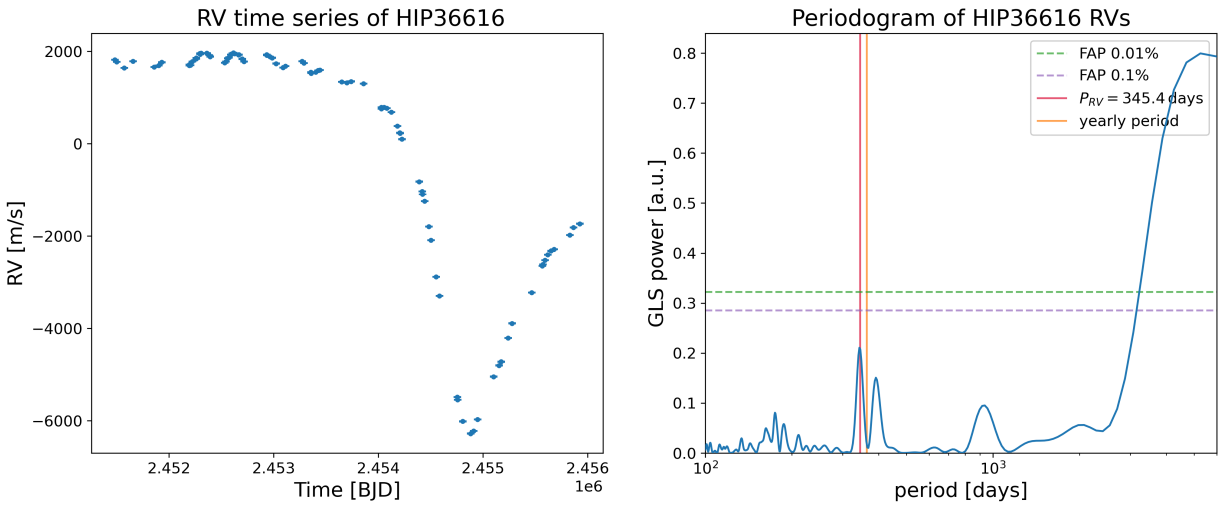

Figure 30: Periodograms for the RV time series of HIP36616.

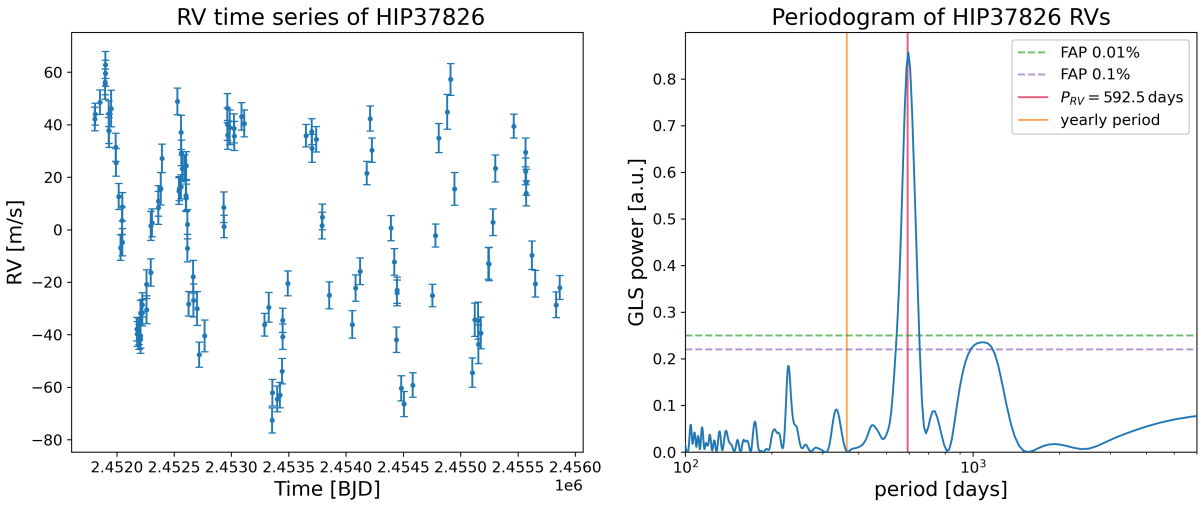

Figure 31: Periodograms for the RV time series of HIP37826.

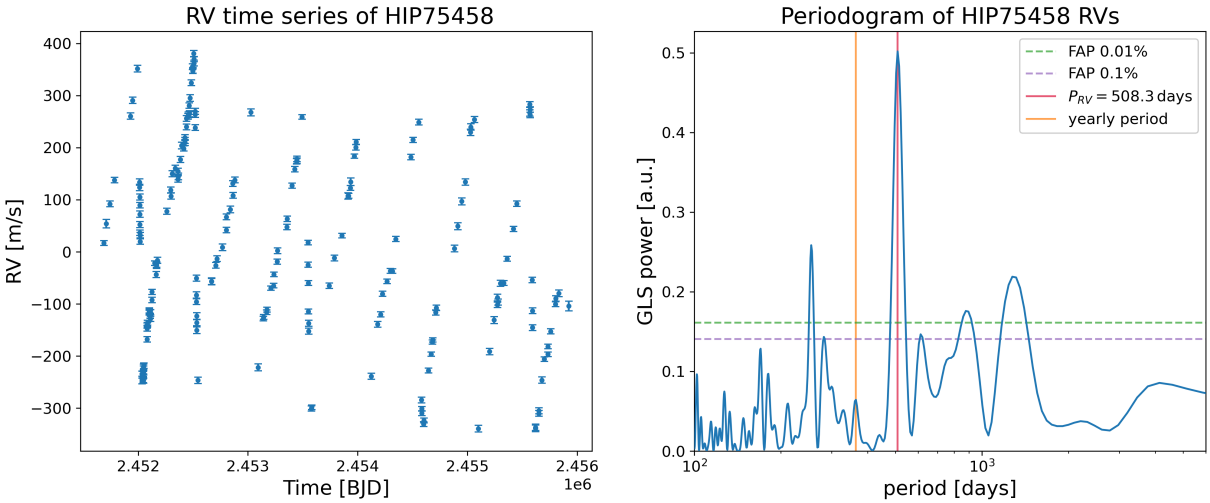

Figure 32: Periodograms for the RV time series of HIP75458.

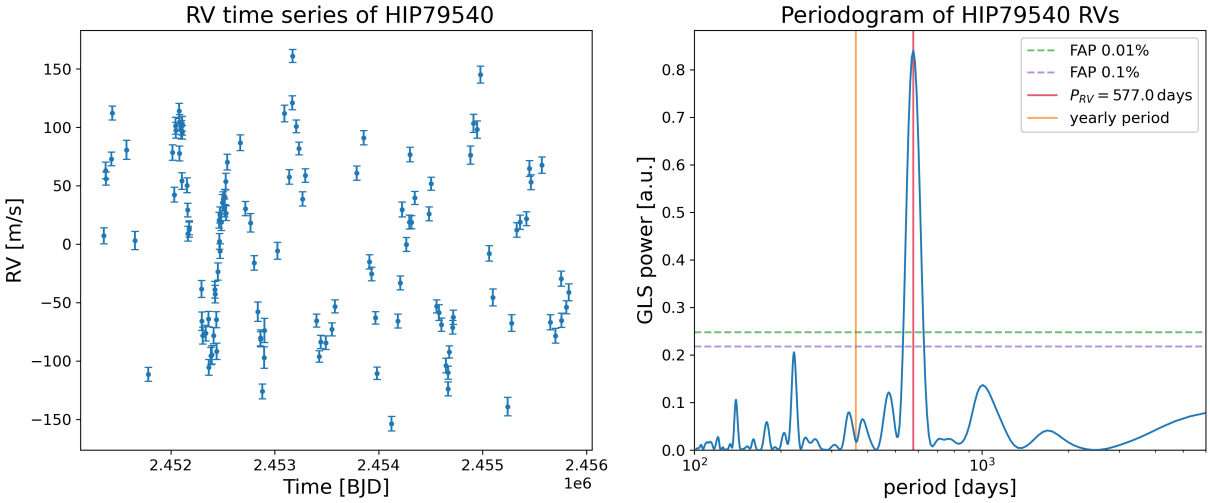

Figure 33: Periodograms for the RV time series of HIP79540.

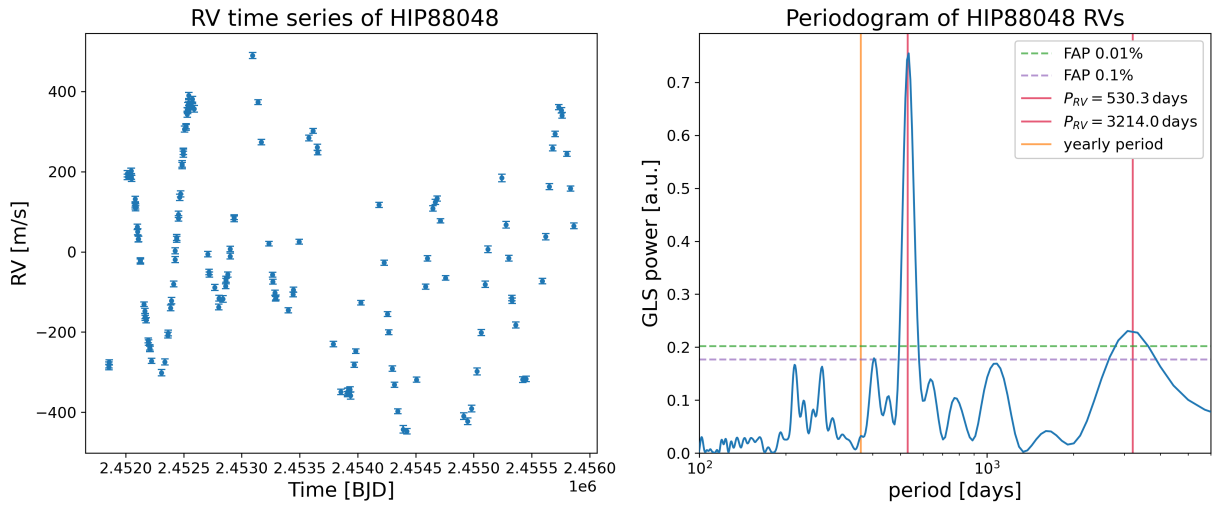

Figure 34: Periodograms for the RV time series of HIP88048.

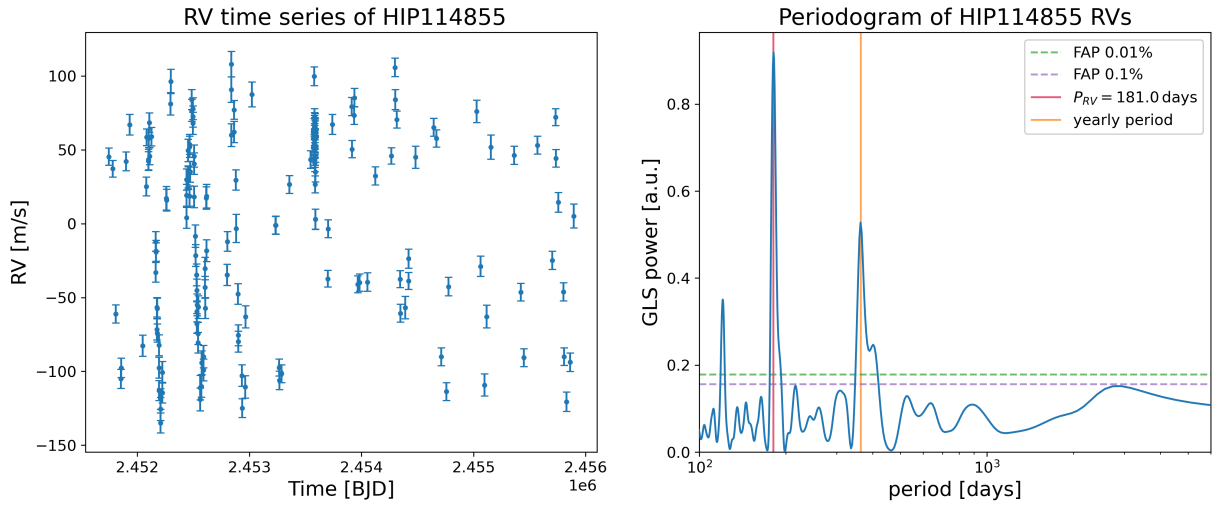

Figure 35: Periodograms for the RV time series of HIP114855.

Declaration

I declare that I have written this thesis by myself and that I have not used any sources or aids other than those indicated.

Heidelberg, the 01.02.2023,

Paul Steinle